

Response to reviewer #1: We'd like to thank the reviewer for their critiques. Our responses to individual comments are below. In addition to the proposed changes to the manuscript, we have added a section (Section 3.6, Figures 11-13) in which the parameterizations for  $D_{pm}$  and  $\sigma$  are tested against real smoke plumes observed at the Mount Bachelor Observatory (contribution by J.R. Laing and D.A. Jaffe).

*This paper studies the effect of coagulation on particle diameter ( $D_m$ ) and geometric standard deviation ( $\sigma$ ) in biomass burning plumes using a large-eddy simulation model with an online aerosol microphysical module. The topic is timely and the text is well written; however, there are some issues that need to be clarified before this manuscript can be accepted. In my opinion this paper presents a valuable base case for assessing the role of coagulation and condensation in future biomass burning studies.*

#### *Major comments*

*I have two major concerns regarding this study: the lack of organic aerosol (OA) chemistry and that while interpreting the results little attention is placed on plume dilution and its effect on coagulation.*

*Running the simulations as “coagulation-only” limits the usability of the results. For instance, new particle formation has been observed in biomass burning plumes (Hennigan et al., 2012; Vakkari et al., 2014), as well as up to a factor of 4 mass increase during the first few hours (Vakkari et al., 2014). Also a recent study by Konovalov et al. (2015) suggests that accounting for OA volatility can improve model performance significantly, although over a much longer time scale than what is considered here. Therefore, without OA evaporation and condensation, can the parameterisations in this paper be a good starting point for global and regional scale models (c.f. line 37)?*

We agree that in order to simulate the mass of organic aerosol (or total  $PM_{2.5}$ ) in the plumes properly, the dynamic production and/or loss of organic aerosol must be better understood. Our intention was not to claim to the contrary of this, and we had included the following discussion on line 389-394 of our text:

“One of the limitations of the coagulation-only parameterizations derived in this paper is that they do not include the effects of potential condensation/evaporation of organic aerosol on the aged biomass-burning size distribution. Both condensational growth and evaporative loss of OA has been observed previously in chamber studies and the field due to OA production or evaporation from dilution/chemistry (Cubison et al., 2011; Hecobian et al., 2011; Hennigan et al., 2011; Grieshop et al., 2009; Ortega et al., 2013; Jolleys et al., 2015; Vakkari et al., 2014).”

We agree that it is important to expand this discussion to discuss simulations where aerosol mass is a primary focus and have added the following to the lines above: “Thus, in order to predict biomass-burning aerosol mass, and thus the aerosol size distribution, we must understand how OA evolves in biomass-burning plumes.”:

We also have in the text a discussion that a change in diameter through coagulation is different than a change in diameter due to OA condensation/evaporation: “It should be noted, however, that the Dpm growth attributed to OA condensation is not accompanied by a change in particle number (additional OA mass is distributed among existing particles), whereas a similar increase in Dpm growth by coagulation only would have an accompanying decrease in particle number. Thus, the changes to the aerosol size distribution and climatic influence of a size change due to coagulation and condensation are different.”

Our intention was to show that the evolution and variability of the mean/median particle diameter seems to be more dependent on the details of coagulation than condensation/evaporation. For example, if fresh biomass-burning particles have a median diameter of 50 nm, a doubling of OA mass would increase the diameter by 13 nm at most, which cannot explain the sizes of aged biomass-burning particles in the atmosphere. We did not intend to take away the importance of SOA that has a large impact on aerosol direct effects and PM<sub>2.5</sub>/health and a secondary importance for aerosol size and the indirect effect.

Finally, the Pierce group along with Matt Alvarado at AER have been recently funded by NSF to extend this work to include SOA formation into subgrid plume parameterizations of biomass burning. Adding SOA will take significant effort due to its complex nature and variability between plumes, and we did not feel that we had the time to test SOA properly during Kim Sakamoto’s Masters thesis, which ultimately dictated the scope of this work. We hope to have an updated scheme that includes SOA within the next several years that draws upon recent advances of biomass-burning SOA measurements from the lab and field.

*On lines 453-455 it is concluded that SOA formation within the plume has a minor effect compared to coagulation. However, this is based on the assumption that SOA formation does not alter coagulation rate or sigma (lines 388-389). Could you elaborate on the conditions when these assumptions hold? For instance Pierce and Adams (2009) showed that secondary aerosol formation rate is one of the key parameters affecting how large fraction of small particles can grow up to CCN-sizes in new particle formation.*

We have added the following sentence to our text at line 393: “For a 25% growth in diameter from SOA, which may be expected from for a factor of 2 increase in OA mass with a small change in sigma, we expect coagulation rates to stay within about 10% (Seinfeld and Pandis, 2006).”

It is correct that SOA can grow new particles to CCN sizes. However, this requires much more than a factor-of-2 increase in OA mass as might be expected in biomass-burning plumes. For example, a factor-of-8 increase in OA mass due to SOA production is required to grow a 40 nm particle to 80 nm. It is certainly plausible that this level of SOA production occurs in some biomass-burning plumes over longer timescales than recent studies; however, this is beyond the scope of this work.

*My second major concern is related to the effect of plume dilution on the coagulation rate. Coagulation depends strongly on aerosol particle number concentration (as stated on lines 145-146). However, the observed changes in  $D_m$  and  $\sigma$  are not discussed in terms of concentration, but only with respect to the input parameters and a rather arbitrary  $dM/dx$  (aerosol mass in an infinitesimally thin slice of air perpendicular to wind direction). The effect of dilution on coagulation is mentioned only briefly (e.g. lines 324-326), though Figure 4 shows that in most simulations the  $D_m$  and  $\sigma$  change rapidly near emission, but very slowly later on. Is this decrease in the rate of change in  $D_m$  and  $\sigma$  due to plume dilution and subsequent slowing of coagulation rate?*

The aerosol concentration in-plume has two competing reducers: coagulation and plume dilution (both of which we'd expect to contribute to the rate changes in Figure 4). We expect the coagulation rate to slow as coagulation proceeds and number concentration drops (mean particle diameter increases). Plume dilution has a similar effect of reducing number concentration (and slowing coagulation) without a corresponding increase in particle diameter. Which of these factors dominates is primarily dependent on the size of the plume and the stability of the atmosphere. Large-diameter plumes are more resistant to plume dilution than small-diameter plumes. While we do not track dilution rate as a parameter, a lot of the associated variability is captured by the "Fire Area" parameter (large-area fires have larger-diameter plumes). We do not include dilution as an explicit input parameter in our analysis (even though plume dilution does occur in the LES simulations) because dilution is not an inherent property that would be provided by a coarse-grid aerosol model or an emissions inventory (unlike all of the other parameters that we studied), and thus we think it would be generally useless to have "dilution" as an input to a parameterization that will be used in coarse-grid models. We have added the following discussion of the importance of dilution in Line 81-82:

"The coagulation rate is therefore also affected by the rate of plume dilution (through a reduction in  $N$ ), itself a function of plume size and meteorological conditions."

While  $dM/dx$  and  $dM/dxdz$  are somewhat arbitrary, we wanted a parameter which i) captured a large chunk of both  $D_{pm}$  and  $\sigma$  variability and ii) was dependent on initial conditions only. These parameters only incorporate total aerosol mass loading, and plume vertical and with-wind extent. When  $dM/dv$  (initial concentration) was used in the simple parameterization, it was a slightly worse predictor of  $D_{pm}$  and  $\sigma$  than  $dM/dxdz$ . This is because  $dM/dxdz$  is the product of  $dM/dv$  and the initial plume width; since wider plumes are less susceptible to dilution than narrower plumes,  $dM/dxdz$  captures this plume-width effect while  $dM/dv$  does not. This is discussed in Lines 393-396:

" $dM/dV$  was also tested as a parameter within these simplified parameterization, but did not yield better agreements for either  $D_{pm}$  or  $\sigma$  than  $dM/dxdz$  despite incorporating an additional plume parameter (initial plume  $y$ -extent). This is because  $dM/dxdz$  is the product of  $dM/dV$  and the initial plume width; since wider plumes are less susceptible to dilution than narrower plumes,  $dM/dxdz$  captures this plume-width effect while  $dM/dV$  does not."

*How does Figure 4 look like if you colour it with concentration instead of  $dM/dx$ , or plot*

*Dm and sigma against concentration? The dM/dx takes into account only dilution along the wind direction, not dilution due to vertical or cross-wind mixing.*

Figure 4 does not look qualitatively different if either  $dM/dxdz$ ,  $dM/dx$ , or  $dM/dv$  (concentration) are used (see attached). We chose  $dM/dx$  as it was the simplest parameter in which the  $D_m$  plot shows a qualitative trend. We have updated the figure to  $dM/dxdz$  instead of  $dM/dx$  to illustrate the stability of this trend when accounting for dilution in the vertical. Initial concentration ( $dM/dV$ ) was not used for consistency with Figures 9-10 where  $dM/dV$  is not an improvement over  $dM/dxdz$  in the simple parameterization (for the reasons stated above) despite requiring more fire information.

*Can you identify a range (time and space), where coagulation can cause significant changes in the size distribution and after which the plumes become so diluted that coagulation slows down? How would this turning point depend on the initial concentration (emissions) and the meteorological conditions (turbulent mixing) during transport?*

Coagulation rates are always slowing down in plumes (proportional to the square of number concentration), so we would need define that it slows down to a subjectively chosen rate. Whether or not a chosen cutoff rate is appropriate depends on the timescale that one cares about, which depends on the modeling application. Since this answer also depends on all of the input factors studied here, the answer is not straightforward and is out of the scope of this paper.

*The background aerosol is assumed to be negligible compared to the plume and is set to zero (lines 176-179). However, in ambient air measurements this assumption cannot be made – see e.g. Yokelson et al. (2009). Have you verified that your plumes are so concentrated even after 200km transport that this assumption still holds? When will coagulation rate with the background aerosol become similar to coagulation within the biomass burning mode?*

At the point where the plumes are diluted to ambient-air concentrations, subgrid processing is no longer different from standard grid-size processing and model schemes are sufficient (no parameterization is needed). We have added an explanation of this at Line 178:

“In cases where the plume dilutes to similar concentrations to the ambient background, subgrid-plume coagulation schemes are no longer necessary, and grid-resolved coagulation will properly account for coagulation.”

*How is turbulent mixing handled in the simulations? Table 1 (page 23) lists “Mixing depth of aerosol layer” as an input parameter, yet on line 214 “mixing depth” is calculated from the simulated vertical profile of aerosol mass. Is this related to mixed layer height (e.g. height of convective planetary boundary layer)?*

SAM calculates turbulence explicitly in the LES using thermodynamic profiles and surface heat/momentum fluxes. There is no assigned PBL in SAM, though it can be calculated from the

resulting profiles. We have used “mixing depth” and “injection height” to refer to the aerosol layer and *not* the convective planetary boundary layer in general (we do not explicitly calculate it anywhere).

*Injection height* is the height at which the biomass-burning aerosol is emitted into the SAM-LES gridboxes after initialization, after which it is subject to turbulent mixing within the model. Depending on meteorological factors, this initialized aerosol layer can remain stable above the PBL or be mixed down through the PBL to the ground (see revised Figure 3). *Mixing depth* is the term used to describe the height extent of the aerosol layer after it is mixed in the LES (at a given point in the LES simulation) to the final time/distance of the simulation, which may vary significantly from the injection height and/or PBL height.

We have changed Line 153 to emphasize our definition of mixing depth:

“...and aerosol mixing depth (hereafter referred to as *mixing depth*; the vertical extent of the aerosol plume)”.

Table 1 has been changed to “Mixing Depth” only for consistency with this definition.

*If Figure 3 is a representative sample of the simulations it seems as if majority of the plumes are not in the mixed layer but above it, as they do not reach the surface. Again, I would expect the turbulent mixing in convective PBL (or the lack of convective mixing in free troposphere or the residual layer) to have a significant effect on plume dilution and therefore the coagulation rate. Is it so?*

*Line 824, Figure 3 Please provide a legend for the lines (indicating input and meteorological parameters).*

We chose our 6 profiles at random for the Figure 3. For 5 of the 6 these cases, the initial height at which we put the plume in the SAM-TOMAS simulation was not in the mixing boundary layer in the model (which is calculated independently by SAM-TOMAS using the meteorological and surface conditions that were randomly chosen for each case). Some simulations were at night where the mixing layer was very small <100m and other cases the injection heights were higher than the daytime mixing layer. We do not expect this to have a great impact on our results as the results should be most sensitive to the depth of the layer the plume mixes to and not whether the plume touches the ground or not.

SAM-TOMAS incorporates a multitude of meteorological parameters (e.g. atmospheric stability) for each simulation in addition to the 7-inputs we varied. Instead of citing specific simulations, we simplified Figure 3 to two representative SAM-TOMAS vertical profiles - one showing the case where the aerosol plume mixes down to the ground through the mixing layer, and one where the plume remains suspended at the injection height throughout the simulation.

The following caption now accompanies Figure 3:

“Final vertical profiles for two representative SAM-TOMAS simulations after four hours, normalized to individual aerosol load and averaged horizontally across the domain. The black profile shows a simulation where the aerosol fully mixed through the boundary layer to the ground, while the red profile shows a simulation where the aerosol plume still stable at the emission injection layer.”

Minor comments:

*Line 69-71 There are some more recent studies which you might want to look up. For instance Akagi et al. (2012), Hennigan et al. (2012), Ortega et al. (2013), Vakkari et al. (2014), Jolleys et al. (2015), Konovalov et al. (2015) and May et al. (2015) come to my mind.*

These references have been added to the appropriate lines with the exception of Ortega et al. (2013), which was already cited at these lines. Konovalov et al. (2015) was added to Section 3.5:

“Konovalov et al. (2015) has emphasized the importance of OA simulation in modeling in long-range (>1000 km) plume evolution.”

*Line 382-385 Also for this statement some more recent references could be considered.*

More recent studies have been appended.

*Line 71 “This SOA condenses onto existing particles causing growth of the aerosol size distribution.” Please reconsider this statement as there are observations of new particle formation in biomass burning plumes (Hennigan et al., 2012; Vakkari et al., 2014).*

We have added the following discussion of new-particle formation in biomass-burning plumes in lines 71-74:

“This SOA can condense onto existing particles causing growth of the aerosol size distribution. It can also spur new-particle formation in biomass-burning plumes as has been observed in lab studies (Hennigan et al., 2012) and field campaign analyses (Vakkari et al., 2014).”

And in Lines 233-235:

“We do not address new-particle formation in biomass-burning plumes in this work. In plumes where new-particle formation in biomass-burning plumes occurs, our parameterizations will underestimate the number of particles and overestimate the mean diameter of the plume particles.”

*Line 153 “Mixing depth had a range of 150-2500 m” but Table 1 (page 23) gives “Mixing depth” limits as 120 m and 2500 m. Which one is it?*

The mixing-depth limit is 150m, and we have updated Table 1.

*Line 169-170 “The algorithm simulated the size distribution across 15 logarithmically-spaced size bins spanning 3 nm-10  $\mu\text{m}$ .” This leaves quite few bins for the size range of interest. Can coarse size resolution become an issue for the coagulation calculation?*

There are 10 bins between 10 nm and 1  $\mu\text{m}$  capture the area of biomass-burning aerosol emission and growth. There are only two bins above 1  $\mu\text{m}$  for coarse aerosol. As we track two independent moments (number and mass) within each bin, the model fidelity is much higher than single-moment schemes with similar resolution. The TOMAS microphysics algorithm has been evaluated in Lee and Adams, (2012) and it generally captures the processes similarly to higher-resolution versions of the model. We now clarify the bin structure: “The algorithm simulated the size distribution across 135 logarithmically -spaced size bins spanning 3 nm-1  $\mu\text{m}$  with 2 additional bins spanning 1-10  $\mu\text{m}$ .”

The coarse size resolution can have an impact on the sigma calculation of the mode near smaller modal sizes ( $\sim 1.32$ ) where the distribution is less than a single bin-width. This is discussed in lines 263-265.

*Line 191-192 “We ran 100 SAM-TOMAS simulations at 500 m x 500 m horizontal resolution (total horizontal extent = 100 km),” but Figure 4 x-axis extends to > 200 km. I assume these are the same data because on lines 244-245 it is stated that “Figure 4 shows the  $D_{pm}$  (panels a and c) and  $\sigma$  (panels b and d) as a function of distance for each of the 100 SAM-TOMAS simulations used to train the emulator (Sect. 3.2).” What was the horizontal extent?*

By “total horizontal extent” we were referring to the cross-wind (y-direction) extent, not the with-wind (x-direction) extent as plotted in Figure 4. Lines 190-196 have been clarified to:

“We ran 100 SAM-TOMAS simulations at 500 m x 500 m horizontal resolution (total cross-wind (y-direction) horizontal extent = 100 km), and constant 40 m vertical resolution (total vertical extent = 4 km)... The output from each SAM-TOMAS simulation was recorded at four different times (400 total time slices across 100 simulations) as the plume progressed along the with-wind (x-direction) axis.”

*Line 871, Figure 4 There are so many overlying lines that it is getting difficult to read. Please consider if you can clarify it.*

We like that Figure 4 shows the evolution of diameter and sigma across all of our simulations so that the reader can see what variability is captured by our simulations. We dedicate the rest of the paper to generalizing the results, so we prefer to keep Figure similar (though we have updated to use  $dM/dxdz$  rather than  $dM/dx$ ).

Response to reviewer #2: We'd like to thank the reviewer for their critiques. Our responses to individual comments are below. In addition to the proposed changes to the manuscript, we have added a section (Section 3.6, Figures 11-13) in which the parameterizations for  $D_{pm}$  and  $\sigma$  are tested against real smoke plumes observed at the Mount Bachelor Observatory (contribution by J.R. Laing and D.A. Jaffe).

*This paper investigates the influence of coagulation on the particle number size distribution, notably on the mean diameter ( $D_m$ ) and geometric standard deviation ( $\sigma$ ) of a single particle mode, in biomass burning plumes. The work is based on a large number of sophisticated model simulations. The authors investigate how  $D_m$  and  $\sigma$  evolve with time in biomass burning plumes, and how their evolution is related to several parameters associated with primary particle emissions, fire conditions and atmospheric conditions. The authors compare briefly the influence of coagulation to that caused by organic aerosol formation/loss in a plume. The authors finally parameterize their results to a form that is applicable in large-scale modeling frameworks.*

*The is scientifically sound and original. The text is well organized and easy to read (with a couple of minor exceptions mentioned below). The authors are able to explain very well the numerous results obtained from model simulations. I have only a few minor suggestions for revisions.*

*Scientific comments:*

*I have a hard time of understanding Figure 3, even after reading the text on lines 210-213. I recommend that the authors work a bit more to make their message here clearer to readers.*

In response to this comment and a comment by reviewer 1, we have simplified Figure 3 to show only two representative profiles of SAM-TOMAS simulations: one which shows the aerosol plume mixing through the boundary layer to the ground, and a second which shows the plume still suspended at the emission injection height at the end of the simulated run. These are the two “types” of mixing depths possible (to ground through the PBL and suspended).

The Figure 3 caption was updated to reflect the changed figure:

“Final vertical profiles for two representative SAM-TOMAS simulations after four hours, normalized to individual aerosol load and averaged horizontally across the domain. The black profile shows a simulation where the aerosol fully mixed through the boundary layer to the ground with some aerosol trapped in a stable layer above the boundary layer, while the red profile shows a simulation where the aerosol plume still stable at the emission injection layer.”

*Lines 254-255. The authors state that the initial mode mean diameter have little effect on  $D_m$ . I do not get this point when looking at Figures 4a and c: if  $D_m$  is initially large, it seems to typically lead to higher values of  $D_m$  at later plume times compared to cases where  $D_m$  is initially small. Could the authors specify what they mean here?*



We mean to emphasize that the variability in Dpm can mainly be attributed to factors outside of initial Dpm. While those simulations with higher initial diameters do climb to higher final diameters than others, the final Dpm variability is not principally driven by starting diameter. As the dominant Dpm variability factors form a discussion in Section 3.3, we have removed this line to alleviate confusion.

*Line 390: Is this correct? Condensation of a non-volatile vapor into a single mode tend to narrow this mode, not widen it, as stated here.*

Your are correct, we wrote the opposite of what we meant. Line 390 is now: "These assumptions are imperfect as irreversible condensation (evaporation) decreases (increases)  $\sigma$ ...".

*The authors analyze shortly the influence OA production/loss on their results (section 3.5), and discuss also the potential effects of cloud processing (lines 463-469). This is clearly sufficient for these two processes in this paper. However, the authors do not mention at all new particle formation (NPF) that has been estimated to be a frequent process in biomass burning plumes. NPF might have notable effects on aerosol size distribution, and thereby on both Dm and Sigma, in evolving biomass burning plume. The authors should spend at least a few lines on discussing the relevance of this process in biomass burning plumes and on the potential effects of NPF on their results.*

We have changed the following discussion of SOA pathways in Section 1.1 (Lines 77-79):

"This SOA can condense onto existing particles causing growth of the aerosol size distribution. It can also spur new-particle formation in biomass-burning plumes as has been observed in lab studies (Hennigan et al., 2012) and field campaign analyses (Vakkari et al., 2014)."

We have added the following lines to our methods:

"We do not address new-particle formation in biomass-burning plumes in this work. In plumes where new-particle formation in biomass-burning plumes occurs, our parameterizations will underestimate the number of particles and overestimate the mean diameter of the plume particles."

*Technical issues:*

*Line 265: Figures 5 shows Sigma versus Dm rather than Dm versus Sigma.*

*Line 382: "..OA has been. . ."*

These have been corrected in text.

# 1 The evolution of biomass-burning aerosol size distributions due to 2 coagulation: dependence on fire and meteorological details and 3 parameterization

4 |  
5 | K.M. Sakamoto<sup>1</sup>, [J.R. Laing<sup>2</sup>](#), R.G. Stevens<sup>3</sup>, [D.A. Jaffe<sup>2,4</sup>](#), and J. R. Pierce<sup>1,5</sup>  
6

7 | [1] Colorado State University, Fort Collins, CO, USA

8 | [\[2\] University of Washington-Bothell, Bothell, WA, USA](#)

9 | [\[3\] University of Leeds, Leeds, UK](#)

10 | [\[4\] University of Washington, Seattle, WA, USA](#)

11 | [\[5\] Dalhousie University, Halifax, NS, Canada](#)  
12

13 | Corresponding author: J.R. Pierce ([jeffrey.pierce@colostate.edu](mailto:jeffrey.pierce@colostate.edu))  
14

## 15 Abstract

16 Biomass-burning aerosols have a significant effect on global and regional aerosol climate forcings. To  
17 model the magnitude of these effects accurately requires knowledge of the size distribution of the  
18 emitted and evolving aerosol particles. Current biomass-burning inventories do not include size  
19 distributions, and global and regional models generally assume a fixed size distribution from all  
20 biomass-burning emissions. However, biomass-burning size distributions evolve in the plume due to  
21 coagulation and net organic aerosol (OA) evaporation or formation, and the plume processes occur on  
22 spacial scales smaller than global/regional-model grid boxes. The extent of this size-distribution  
23 evolution is dependent on a variety of factors relating to the emission source and atmospheric  
24 conditions. Therefore, to account for biomass-burning aerosol size in global models accurately requires  
25 an *effective* aerosol size distribution that accounts for this sub-grid evolution and can be derived from  
26 available emissions-inventory and meteorological parameters.

27 In this paper, we perform a detailed investigation of the effects of coagulation on the aerosol size  
28 distribution in biomass-burning plumes. We compare the effect of coagulation to that of OA  
29 evaporation and formation. We develop coagulation-only parameterizations for effective biomass-

30 burning size distributions using the SAM-TOMAS large-eddy simulation plume model. For the most-  
31 sophisticated parameterization, we use the Gaussian Emulation Machine for Sensitivity Analysis  
32 (GEM-SA) to build a parameterization of the aged size distribution based on the SAM-TOMAS output  
33 and seven inputs: emission median dry diameter, emission distribution modal width, mass emissions  
34 flux, fire area, mean boundary-layer wind speed, plume mixing depth, and time/distance since  
35 emission. This parameterization was tested against an independent set of SAM-TOMAS simulations,  
36 and yields  $R^2$  values of 0.83 and 0.89 for  $D_{pm}$  and modal width, respectively. The size distribution is  
37 particularly sensitive to the mass emissions flux, fire area, wind speed, and time, and we provide  
38 simplified fits of the aged size distribution to just these input variables. The simplified fits were tested  
39 against eleven aged biomass-burning size distributions observed at the Mt. Bachelor Observatory in  
40 August 2015. The simple fits captured over half of the variability in observed  $D_{pm}$  and modal width  
41 even though the freshly emitted  $D_{pm}$  and modal widths were unknown. These fits may be used in global  
42 and regional aerosol models. Finally, we show that coagulation generally leads to greater changes in the  
43 particle size distribution than does OA evaporation/formation using estimates of OA production/loss  
44 from the literature.

## 45 **1. Introduction**

### 46 ***1.1 Biomass-burning aerosols***

47 Biomass burning (including wildfires, prescribed fires, and agricultural fires) releases significant  
48 amounts of gas- and particle-phase species to the atmosphere (Andreae and Merlet, 2001; Reid et al.,  
49 2005). The particle-phase emissions are composed primarily of a mixture of organic aerosol (OA) and  
50 black carbon (BC) with some inorganic species (e.g. potassium), and the ratios of these species depend  
51 on the source fire conditions (Capes et al., 2008; Carrico et al., 2010; Cubison et al., 2011; Hecobian et  
52 al., 2011; Hennigan et al., 2011; Reid et al., 2005). These aerosols affect the global radiation budget  
53 through the indirect and direct aerosol effects (Boucher et al., 2013). The smoke particles themselves  
54 are able to act as cloud condensation nuclei (CCN) and increase cloud albedo and lifetime (indirect  
55 aerosol effect; Lee et al., 2013; Pierce et al., 2007; Spracklen et al., 2011) as well as  
56 scattering/absorbing incoming solar-radiation directly (direct aerosol effect; Alonso-Blanco et al., 2014;  
57 Boucher et al., 2013; Haywood and Boucher, 2000; Jacobson, 2001).

58 Particle size has a significant effect on the magnitude of both the direct and indirect aerosol

59 effects (Lee et al., 2013; Seinfeld and Pandis, 2006; Spracklen et al., 2011). The composition and  
60 diameter of the particles affect their absorption/scattering efficiencies, which dictate the amount of  
61 solar radiation absorbed/scattered per emitted mass of particles (Seinfeld and Pandis, 2006). Particle  
62 diameter and hygroscopicity determine the particles' ability to act as a CCN and influence cloud  
63 processes, and the total number of emitted particles increases with decreased particle size if total mass  
64 emissions are fixed. Spracklen et al., (2011) found that a reduction by a factor of two in particle size for  
65 all carbonaceous aerosols (for a fixed total aerosol mass) resulted in a ~300% increase in the cloud  
66 albedo indirect effect globally, as more particles were available to act as CCN. Lee et al., (2013)  
67 determined that CCN concentrations in the GLOMAP model were very sensitive to uncertainties in  
68 biomass-burning emission diameter on both the regional and global scale (its attributable CCN  
69 uncertainty ranked third of 28 factors tested globally). Therefore, to ascertain the role of biomass-  
70 burning aerosols in climate forcings accurately, biomass-burning size distributions must be well  
71 represented in aerosol-climate models.

72 Size distributions are subject to physical and chemical processing in the plume. The formation of  
73 secondary organic aerosol (SOA) has been observed in lab studies of biomass-burning aerosol  
74 (Cubison et al., 2011; Grieshop et al., 2009; Hennigan et al., 2011; Heringa et al., 2011; Ortega et al.,  
75 2013) and in field campaigns (DeCarlo et al., 2010; Lee et al., 2008; Reid et al., 1998; Yokelson et al.,  
76 2009). This SOA can condenses onto existing particles causing growth of the aerosol size distribution.  
77 It can also spur new-particle formation in biomass-burning plumes as has been observed in lab studies  
78 (Hennigan et al., 2012) and field campaign analyses (Vakkari et al., 2014). Conversely, recent lab and  
79 field studies have characterized primary organic aerosol (POA) as semi-volatile, with plume dilution  
80 allowing the evaporation of organic aerosol from particles (Huffman et al., 2009; Cubison et al., 2011;  
81 May et al., 2013, 2015; Jolleys et al., 2015,–). The cumulative net effects of OA production/loss within  
82 biomass-burning plumes has been found to be highly variable from fire to fire (Akagi et al., 2012;  
83 Hennigan et. al, 2011).

84 \_\_\_\_\_ Coagulation is also important for size-distribution evolution as it reduces particle number and  
85 shifts the distribution to larger sizes. Coagulation rates are proportional to the square of the particle  
86 number concentration (all else remaining fixed), so the high number concentrations in biomass-burning  
87 plumes relative to background can lead to rapid coagulation growth of the size distribution. The  
88 coagulation rate is therefore also affected by the rate of plume dilution (through a reduction in N), itself  
89 a function of plume size and meteorological conditions. The rate and magnitude of the aerosol growth

90 caused by these combined processes is a function of aging time, emission source characteristics,  
91 aerosol properties at emission, and atmospheric conditions.

92         These condensation/evaporation and coagulation aging processes affect both the composition and  
93 size of the aerosol size distribution – both properties that influence the extent to which smoke particles  
94 affect climate. While fresh smoke is generally composed of fine particles between 20-60 nm in  
95 diameter (Levin et al., 2010), condensation and coagulation cause rapid aerosol growth to larger sizes  
96 (over 100 nm) on timescales of often less than 24 hrs (Janhäll et al., 2010). However, Janhäll et al.,  
97 (2010) found the observed geometric mean diameter of aged biomass-burning particles varied between  
98 170-300 nm, with geometric standard deviations (hereafter referred to as “modal width”) between 1.3-  
99 1.7 with significant dependence on fuel type and modified combustion efficiency. It is currently unclear  
100 to what extent these factors and others drive the variability in aged size distributions.

101         As stated earlier, an accurate representation of aged biomass-burning aerosol size is necessary for  
102 predictions of aerosol climate effects in regional and global models (Lee et al., 2013). Current wildfire  
103 inventories are mass-based (neglecting aerosol size data), and thus regional and global models used for  
104 aerosol-climate effects generally specify fixed, “aged” size distributions that do not account for sub-  
105 grid processing of the emitted particles (Reid et al., 2009; van der Werf et al., 2010; Wiedinmyer et al.,  
106 2011). Any variability in the biomass-burning size distribution due to fire or emissions characteristics  
107 and meteorology are not accounted for, nor is it clear what the best “aged” size distribution to use is in  
108 these models.

109         In this paper, we perform a detailed investigation of coagulation in biomass-burning plumes and  
110 compare to the effects of OA evaporation and formation. We investigate the factors that influence  
111 coagulation growth of the particles in the plume. These factors include fire area, particle-emissions  
112 mass flux, particle-emissions size, and meteorological conditions. We create parameterizations of  
113 varying degrees of complexity for median dry diameter ( $D_{pm}$ ) and lognormal modal width ( $\sigma$ ) of the  
114 aged biomass-burning size distributions as a function of these input parameters, based on detailed  
115 numerical simulations using a large-eddy model with embedded aerosol microphysics (SAM-TOMAS).  
116 Finally, we compare the effect of coagulation on the aerosol size distribution to that of OA  
117 production/evaporation.

118         We describe the parameterization building process, including the use of a Gaussian emulator, in  
119 Sect. 2. A discussion of input and output ranges, processing, and constraints of the parameters we have

120 chosen is provided in Sect. 2.1. We discuss the SAM-TOMAS model and the emulation process in Sect.  
121 2.2-2.3. Sections 3.1-3.2 contain the results of the SAM-TOMAS model and the emulator. We discuss  
122 emulator sensitivities to the inputs in Sect. 3.3 and present a series of simplified fit equations for the  
123 effective size distributions in Sect. 3.4. We discuss the effects of potential OA production/loss on our  
124 size distribution estimates in Sect. 3.5. The simplified-fit equations are tested against biomass-burning  
125 plumes observed at the Mt. Bachelor Observatory in Sect. 3.6. Finally, we conclude in Sect. 4,  
126 including future plans for testing the parameterization and known existing limitations.

127

## 128 **2. Methods**

129 Figure 1 provides an overview of our methods that will be described in detail in the subsections below.  
130 In short, we used a Large-Eddy Simulation model, the System for Atmospheric Modelling (SAM;  
131 Khairoutdinov and Randall, 2003), with the online aerosol microphysics module, TwO Moment  
132 Aerosol Sectional (TOMAS, Adams and Seinfeld, 2002; Stevens et al., 2012) to simulate the evolution  
133 of the biomass-burning aerosol size distribution by coagulation across a wide range of emission and  
134 meteorological conditions. We used the SAM-TOMAS size distributions to build parameterizations to  
135 predict aged  $D_{pm}$  and  $\sigma$  using: (1) a statistical emulator of the SAM-TOMAS model itself and (2)  
136 simplified fits to the SAM-TOMAS output data. The statistical emulator was built by the Gaussian  
137 Emulation Machine for Sensitivity Analysis (GEM-SA), and we used the emulator and SAM-TOMAS  
138 data to determine the relative importance of various inputs to shaping the aged size distribution.

### 139 ***2.1 Investigated factors that may lead to variability in aged size distributions***

140 We investigated seven parameters that may affect the aging of the biomass-burning aerosol size  
141 distribution. These can be divided into those representing the initial lognormal-mode size parameters  
142 ( $D_{pm0}$ ,  $\sigma_0$ ), fire conditions (mass flux, fire area), atmospheric conditions (wind speed, plume mixing  
143 depth), and time. Each of these parameters is generally available in large-scale aerosol models, which  
144 means a parameterization for aged biomass-burning size distributions based on these parameters may  
145 be used in these models. Table 1 lists these input parameters and the ranges of values tested in this  
146 work.

147 We assumed that the initial size distributions were a single lognormal mode (described by dry  
148 median diameter,  $D_{pm}$ , and modal width,  $\sigma$ ), which is sufficient when representing both fresh and aged  
149 observed biomass-burning size distributions (Capes et al., 2008; Janhäll et al., 2010; Levin et al., 2010;  
150 Sakamoto et al., 2015). The initial size-distribution parameters specify the median dry diameter ( $D_{pm0}$ )  
151 and modal width ( $\sigma_0$ ) of the freshly emitted aerosol distribution. We varied these parameters between  
152 20-100 nm for  $D_{pm0}$  and 1.2-2.4 for  $\sigma_0$ . The large ranges are due to variability in combustion efficiency  
153 and fuel-type factors as seen in lab and observational studies (Janhäll et al., 2010; Levin et al., 2010).

154 Fire area, mass flux, wind speed and [aerosol mixing depth](#) ([hereafter referred to as \*mixing\*](#)  
155 [depth](#); the vertical extent of the aerosol plume) all affect the aerosol number concentration ( $N$ ) within  
156 the plume, which in turn affects the coagulation rate (proportional to  $N^2$ ). In our simulations, we  
157 constrained mass flux to  $2 \times 10^{-8}$  -  $5 \times 10^{-6}$  kg m<sup>-2</sup> s<sup>-1</sup> using approximate maximum and minimum values  
158 of summed black carbon and organic carbon flux (BC+OC) found in the Global Fire Emissions  
159 Database ver. 3 (GFED3; van der Werf et al., 2010; available from <http://www.globalfiredata.org>). Fire  
160 area ranged from 1 - 49 km<sup>2</sup> (simulated as a square), which was found to represent the range of fire  
161 sizes in GFED3. Boundary layer wind speed varied between 2 m s<sup>-1</sup> and 20 m s<sup>-1</sup> and was based on  
162 ranges in the National Center for Environmental Prediction (NCEP) North American Regional  
163 Reanalysis (NARR) meteorology (Mesinger et al., 2006) during the fire season (specifically, July,  
164 2010). Mixing depth had a range of 150-2500 m (based on SAM-TOMAS output; see Sect. 2.2).

165 The aging time was the final input parameter, and we used 5 hr (300 min) as an upper time  
166 bound due to this being a typical timescale for transport across large global model gridboxes.

## 167 **2.2 The SAM-TOMAS model**

168 We used the SAM-TOMAS model to simulate the evolution of biomass-burning aerosol size  
169 distributions due to coagulation across the range of input parameters described above. SAM  
170 (Khairoutdinov and Randall, 2003) is a dynamical large-eddy simulation (LES) model, which has  
171 previously been used to model emissions plumes (Lonsdale et al., 2012; Stevens et al., 2012; Stevens  
172 and Pierce, 2013). We ran the model in Lagrangian 2D mode (Stevens and Pierce, 2013), in which a  
173 wall oriented normal to the mean boundary layer wind moves at the mean boundary-layer wind speed.  
174 This moving wall tracks the radial dispersion of a plume as it travels downwind (Fig. 2). This 2D mode  
175 is computationally efficient compared to the full 3D model with minor differences due to axial plume



176 symmetry (Stevens and Pierce, 2013).

177 The size distributions of the aerosol particles in SAM were simulated using the Two Moment  
178 Aerosol Sectional (TOMAS; Adams and Seinfeld, 2002) microphysical scheme embedded into SAM.  
179 The algorithm simulated the size distribution across 135 logarithmically spaced size bins spanning 3  
180 nm-10  $\mu\text{m}$  with 2 additional bins spanning 1-10  $\mu\text{m}$ . The aerosol size distribution was tracked via two  
181 independent moments for each bin of the size distribution (mass and number). TOMAS calculated  
182 coagulation explicitly in each grid cell assuming a Brownian diffusion kernel (Seinfeld and Pandis,  
183 2006). Our SAM-TOMAS simulations included only coagulation, and particles were assumed to be a  
184 single species (no differentiating between BC and OA). The SAM-TOMAS model had previously been  
185 tested against observations in Stevens et al. (2012) and Lonsdale et al. (2012) for power plant plumes.

186 We set background aerosol concentrations to zero as the biomass-burning aerosol  
187 concentrations emitted into SAM-TOMAS were orders of magnitude larger than those present in a  
188 remote background location, and as such the lack of background aerosol would have had an  
189 insignificant effect on the rate of in-plume coagulation processing. In cases where the plume dilutes  
190 to similar concentrations to the ambient background, subgrid-plume coagulation schemes are no longer  
191 necessary, and grid-resolved coagulation will properly account for coagulation. The biomass-burning  
192 aerosol was assumed to have a constant density of 1400 kg m<sup>-3</sup> as primarily a mix of organic  
193 compounds, thus we do not consider how changes in BC/OA composition may affect density and  
194 coagulation rates. The hygroscopicity of the aerosol particles was set to zero, allowing no water uptake.  
195 This assumption is not true of real world biomass-burning aerosol and has been characterized in other  
196 works finding hygroscopicities of fresh ( $\kappa=0.02-0.8$ ; Petters et al., 2009) and aged smoke ( $\kappa=0.1-0.3$ ;  
197 Engelhart et al., 2012) with a strong dependence on fuel type. In terms of their effect on the size  
198 distribution, a constant  $\kappa$  across all particle sizes has the simple effect of increasing the effective  
199 diameter of the particles via water uptake by a scalar factor. This initial increase should only have a  
200 relatively minor effect on the final dry  $D_{\text{pm}}$  or  $\sigma$  of the plume after coagulation processing as the mean  
201 coagulation rates are relatively insensitive to the size shifting of a particle population (Seinfeld and  
202 Pandis, 2006; Stuart et al., 2013).

203 We ran 100 SAM-TOMAS simulations at 500 m x 500 m horizontal resolution (total cross-wind  
204 (y-direction) horizontal extent = 100 km), and constant 40 m vertical resolution (total vertical extent =  
205 4 km). This resolution accommodated the chosen plume parameters (see Sect. 2.1). The model was run  
206 with a master timestep of 2 seconds (varied internally for accuracy in the coagulation calculation) for a

207 duration of 5 model hours (300 minutes). The output from each SAM-TOMAS simulation was  
208 recorded at four different times (400 total time slices across 100 simulations) as the plume progressed  
209 along the with-wind (x-direction) axis.

210 The seven inputs to the SAM-TOMAS model were constrained to capture a range of biomass-  
211 burning characteristics in realistic scenarios and are summarized in Table 2. The ranges of values used  
212 for  $D_{pm0}$ ,  $\sigma_0$ , fire area and mass flux are the same as those listed in Table 1. The meteorological fields  
213 were supplied by NCEP reanalysis meteorology from over North America (land only, lat: 30° - 70° N,  
214 lon: 70° -135° W) during the July 2010 fire season. The SAM-TOMAS wall speed was set equal to the  
215 mean boundary layer wind speed from NCEP. We filtered these inputs by requiring wind speed  $> 2 \text{ m s}^{-1}$   
216 to eliminate stagnation situations over the source. The injection height (lower bound) and injection  
217 depth of the aerosol were specified at between 50-1500 m and 500-2000 m respectively. No emission  
218 injection parameterization (e.g. Freitas et al., 2007) was used as we were only trying to capture a range  
219 of mixing depths for our aging calculation, and the absolute height was relatively unimportant. All the  
220 SAM-TOMAS simulation inputs were chosen using semi-random Latin hypercube sampling across the  
221 ranges listed above (Lee et al., 2012). The results of the full SAM-TOMAS simulation set are  
222 summarized in Sect. 3.1.

223 We calculated the time-dependent mixing depth of the plume from vertical profiles averaged  
224 horizontally across the entire simulation wall at each time slice. Figure 3 shows a sample of sixtwo  
225 vertical profiles from different SAM-TOMAS simulations. The mixing depth was defined as the range  
226 of altitudes where the aerosol mass was greater than half of the peak aerosol mass:

227 
$$\text{mixing depth} = \Delta_{\text{alt } 50\% \text{ peak aerosol mass}}$$

228 In cases where the plume mixed down to the ground, the lower altitude bound was defined as 0  
229 m. Runs with mixing depths greater than 2500 m were excluded to ensure that the plume did not reach  
230 the model top. In addition to mixing depth,  $D_{pm}$  and  $\sigma$  were calculated for each of the SAM-TOMAS  
231 time slices from the first and third integrated moments of the size distribution as detailed by Whitby et  
232 al. (1991).

233 We do not address new-particle formation in biomass-burning plumes in this work. In plumes  
234 where new-particle formation in biomass-burning plumes occurs, our parameterizations will  
235 underestimate the number of particles and overestimate the mean diameter of the plume particles.

## 236 **2.3 Emulation of the SAM-TOMAS output**

237 As running the full SAM-TOMAS model is too computationally expensive for implementation in  
238 global aerosol models, we built an offline emulator of the model for use as a parameterization in these  
239 global models. We created the emulator using the Gaussian Emulation Machine for Sensitivity Analysis  
240 (GEM-SA) developed by the Centre for Terrestrial Dynamics\_   
241 (<http://www.ctcd.group.shef.ac.uk/gem.html>). The GEM-SA software uses a Gaussian process to design a  
242 SAM-TOMAS simulator (the emulator) based on the behavior of the known SAM-TOMAS inputs and  
243 outputs (the training data). A complete description of GEM-SA statistics and assumptions can be found  
244 in Kennedy and O'Hagan (2001) and Kennedy et al. (2008). A description of its application as an  
245 estimator in atmospheric-aerosol modelling can be found in Lee et al. (2011). This software was  
246 previously used in sensitivity studies in atmospheric-aerosol (Lee et al., 2011, 2012) and vegetation  
247 models (Kennedy et al., 2008).

248 We used 400 data points from the set of 100 SAM-TOMAS simulations to train the emulator.  
249 GEM-SA assumes that the outputs are a continuous and differentiable function of the inputs to  
250 statistically emulate the model and estimate the SAM-TOMAS output ( $D_{pm}$  and  $\sigma$ ). We used a new set  
251 of completed SAM-TOMAS simulations (624 non-training data points) to test our GEM-SA  
252 parameterization for accuracy relative to SAM-TOMAS (see Sect. 3.2-3.3).

253 The GEM-SA parameterization requires seven input parameters:  $D_{pm0}$ ,  $\sigma_0$ , mass flux, fire area,  
254 wind speed, mixing depth and time, and generates predicted aged  $D_{pm}$  and  $\sigma$  as outputs. These  
255 estimated  $D_{pm}$  and  $\sigma$  describe an aged lognormal aerosol mode incorporating the sub-grid scale  
256 coagulation taking place inside concentrated biomass-burning plumes and can be used in  
257 global/regional models. We have made the GEM-SA parameterization (emulator Fortran subroutine and  
258 input files) available as Supplementary Material.

## 259 **3. Results**

### 260 **3.1 SAM-TOMAS simulation output**

261 Figure 4 shows the  $D_{pm}$  (panels a and c) and  $\sigma$  (panels b and d) as a function of distance for each of the  
262 100 SAM-TOMAS simulations used to train the emulator (Sect. 3.2). The influence of several factors

263 (the distance from the source, emissions mass flux, and fire area) on the final aerosol size distributions  
264 is apparent in the output of SAM-TOMAS simulations. Panels a and b are colored by the emissions  
265 mass flux, whereas panels c and d are colored by  $dM/dx dz$  ( $\text{kg m}^{-2}$ , the amount of aerosol mass in an  
266 infinitesimally thin slice of air perpendicular to the direction of the wind, i.e. mass flux  $\cdot$  fire area /  
267 wind speed/mixing depth). All simulations showed  $D_{pm}$  increasing with distance as coagulation  
268 progressed in each plume. The coloring in panel a shows that  $D_{pm}$  generally increases more rapidly and  
269 to higher values with higher emission fluxes. However, panel c shows that  $dM/dx dz$  appears to be a  
270 better predictor for the increase of  $D_{pm}$  with distance than the emissions flux, and the distance and  
271  $dM/dx dz$  capture much of the variability in  $D_{pm}$ .  ~~$D_{pm0}$  appears to have little influence on  $D_{pm}$  (note,~~  
272 ~~however, that the first points on these plots already include some processing and are not the initial~~  
273 ~~diameters).~~

274 Panels b and d show that  $\sigma$  tends to converge with distance as simulations with large initial  $\sigma$   
275 generally decrease with distance more rapidly than simulations with smaller initial  $\sigma$ . This convergence  
276 happens slowly relative to the times simulated, so the initial  $\sigma$  have a strong influence even at 200 km.  
277 The colors and panels b and d show that  $\sigma$  in high emissions-flux and  $dM/dx dz$  cases converge more  
278 rapidly than low-emissions cases. However, as opposed to the 1.32 modal-width asymptote in the limit  
279 of infinite coagulation found by Lee (1983), the SAM-TOMAS simulations converge to a limit of 1.2-  
280 1.25. This is likely due to the size-distribution bin-spacing in the SAM-TOMAS model, where modal  
281 widths  $<1.32$  are smaller than a single TOMAS size bin width, which results in less accurate fits of  $\sigma$   
282 for smaller  $\sigma$  values.

283 Figure 5 is a scatterplot of  ~~$D_{pm}$  vs  $\sigma$  vs  $D_{pm}$~~  for each point seen in Fig. 4, excepting those at  
284 distances less than 25 km (points close to the emissions source have been removed). The points are  
285 colored by  $dM/dx dz$ . Thus, Fig. 5 shows the results of Fig. 4 panels c and d together but removes the  
286 distance information. At these distances over 25 km,  $D_{pm}$  is relatively well constrained by  $dM/dx dz$   
287 alone, showing that the mean growth by coagulation is strongly influenced by the mass of particles in  
288 the slice of air. On the other hand,  $\sigma$  is unconstrained at low values of  $dM/dx dz$  but more constrained  
289 towards 1.2-1.4 at high values of  $dM/dx dz$ . At high  $dM/dx dz$  values, the convergence towards the  
290 steady-state  $\sigma$  proceeds much more rapidly than at low  $dM/dx dz$  as also shown in Fig. 4d.

291 These SAM-TOMAS results show that  $dM/dx dz$  is a powerful determinant of aged biomass-  
292 burning size. In these tests, we also explored the suitability of  $dM/dx$  (mass flux  $\cdot$  fire area/ wind speed)  
293 and  $dM/dV$  (initial mass concentration). Large mixing depths dilute particle concentrations and reduce

294 coagulation, so we expected that  $dM/dxdz$  may be a better predictor of biomass-burning size-  
295 distribution aging than  $dM/dx$ . However, Fig. 4 and Fig. 5 did not look qualitatively different when  
296 using  $dM/dx$  or  $dM/dV$ . [A comparison of  \$dM/dx\$  vs  \$dM/dxdz\$  vs  \$dM/dV\$  in predicting final size-](#)  
297 [distribution attributes is further discussed in Section 3.4.](#) We quantitatively evaluate the fidelity of  
298  $dM/dx$  and  $dM/dxdz$  as proxies for biomass-burning size-distribution aging in Sect. 3.4. In the  
299 following two subsections, we use the emulator to determine the contribution of the individual inputs to  
300 the changes in simulated  $D_{pm}$  and  $\sigma$ .

### 301 ***3.2 Model parameterization evaluation***

302 We tested the GEM-SA-derived emulator parameterization against additional SAM-TOMAS model  
303 runs that were not used in the fitting of the parameterization, and we show the results in Fig. 6. We use  
304 624 additional SAM-TOMAS-simulated data points that were not used for GEM-SA training in this  
305 evaluation. The emulator parameterization-predicted outputs corresponding to these data points for  $D_{pm}$   
306 and  $\sigma$  are plotted against the SAM-TOMAS  $D_{pm}$  and  $\sigma$ . Predicted  $D_{pm}$  has an  $R^2$  value of 0.83 with a  
307 slope of 0.92. Larger absolute errors in  $D_{pm}$  are found at the larger diameter sizes, but 86% are found  
308 within 10% of the SAM-TOMAS  $D_{pm}$  (76% of predicted  $D_{pm}$  are within 5% of SAM-TOMAS  $D_{pm}$ ).  
309 The small mean normalized bias (MNB) of -0.06 indicates a slight negative bias in the  
310 parameterization. This bias is generally seen towards the higher final  $D_{pm}$  values in the simulations  
311 (>250 nm), which are reached only by the most aged plumes with the heaviest aerosol loads. The  $\sigma$  plot  
312 (Fig. 6b) shows a similar correlation coefficient ( $R^2=0.91$ ) and has a slope of 0.93. The MNB is 0.01  
313 and 77% of the predicted  $\sigma$  points are within 5% of the  $\sigma$  calculated from SAM-TOMAS. The cluster of  
314 points near  $\sigma = 1.2-1.3$  is indicative of the modal width steady-state limit. This limit is not captured by  
315 the  $\sigma$  parameterization, which assumes a smooth function towards even lower  $\sigma$  values.

### 316 ***3.3 Sensitivity of aged size distribution to input parameters***

317 Figures 7 and 8 show the sensitivities of the parameterization outputs ( $D_{pm}$  and  $\sigma$ , respectively) to the  
318 input parameters ( $D_{pm0}$ ,  $\sigma_0$ , mass flux, fire area, wind speed, time, and mixing depth) as determined by  
319 the GEM-SA emulation of the SAM-TOMAS output. (Note that distance was used as the dependent  
320 variable in Fig. 4, while we use time in the emulator. Time can be converted to distance by multiplying  
321 by the wind speed). In every panel, each line shows the change in  $D_{pm}$  (Fig. 7) or  $\sigma$  (Fig. 8) as an input  
322 parameter (e.g.  $D_{pm0}$  in panel a) is varied systematically from its minimum to maximum tested value

323 with a randomly chosen set of the other six input parameters. Each panel contains 100 lines, which  
324 means that 100 sets of the six other input parameters were randomly chosen to make these lines. We  
325 normalize each line by the value of  $D_{pm}$  or  $\sigma$  at the midpoint of the x-axis (i.e. where the input  
326 parameter is at the midpoint of its tested range). For time since emission (panel f) we normalize by the  
327 values at  $t=0$  min instead of at the midpoint of the range. These plots therefore show the percent change  
328 in  $D_{pm}$  or  $\sigma$ ,  $\Delta\%_{output}$ , as each input is changed from its midpoint value (or  $t=0$  min for time), in order to  
329 emphasize the parameterization's output response to each isolated input variable.

330 The  $D_{pm}$  sensitivity plots (Fig. 7) show a number of well-defined responses of  $D_{pm}$  to the inputs.  
331  $D_{pm}$  increases monotonically with increases in mass flux and fire area (Fig. 5b,d), and decreases nearly  
332 monotonically with wind speed. These trends are due to the interrelationships of these inputs with  
333 starting number concentration. These results are consistent with Fig. 4 and Fig. 5, where  $D_{pm}$  increased  
334 with increasing  $dM/dx$  in the SAM-TOMAS simulations. Additionally, the  $D_{pm}$  also decreases  
335 monotonically with mixing depth (albeit more weakly than mass flux, fire area, and wind speed), so  
336  $dM/dxdz$  may also be a good proxy for biomass-burning size-distribution aging (evaluated in Sect. 3.4).  
337 Higher  $dM/dx$  and  $dM/dxdz$  values lead to higher initial number concentration in these plumes, which  
338 drive higher rates of coagulation due the squared dependence of coagulation rate on number  
339 concentrations.

340  $D_{pm}$  also increases nearly monotonically with time (the regions of slight decreases with time  
341 show that the parameterization is not necessarily always physically representative due to the statistical  
342 nature of the fit over the parameter space). The rapid rise in  $D_{pm}$  for time  $<2$  hrs is due to the high  
343 number concentrations ( $N$ ) and coagulation rates near the source. As dilution and coagulation progress,  
344  $N$  decreases and coagulation slows, resulting in a slowing of  $D_{pm}$  increase. Mass flux has the largest  
345 range of output  $D_{pm}$  associated with the input ranges specified here ( $\sim -50\%$  to  $+100\%$ ).

346 The relationship between  $D_{pm}$  and the initial size parameters ( $D_{pm0}$  and  $\sigma_0$ ) is more complicated.  
347 Neither  $D_{pm0}$  nor  $\sigma_0$  show monotonic increases or decreases in  $D_{pm}$  due to changes in either of these  
348 isolated inputs. In general, there is an increasing trend in output  $D_{pm}$  with increasing  $D_{pm0}$ , but for some  
349 cases it decreases. These decreases in  $D_{pm}$  are likely due to (1) decreasing particle number  
350 concentrations with increasing  $D_{pm0}$ , which leads to reduced coagulation rates and (2) imperfections in  
351 the statistical fit of the parameter space. The larger  $\sigma_0$  indicate broader emission size distributions, with  
352 more large particles and small particles. Since coagulation progresses fastest between large and small  
353 particles (as opposed to particles of approximately the same size), this favors higher  $D_{pm}$  at higher  $\sigma$ .

354 However, the initial particle number decreases with increasing  $\sigma$ , which lowers the coagulation rate and  
355 leads to lower  $D_{pm}$ .

356 The emulator-derived  $\sigma$  sensitivities are shown in Fig. 8. Since we expect  $\sigma$  to converge towards  
357 an asymptotic limit with coagulation processing (Fig. 4b,d), we see with those input parameters  
358 associated with higher plume number density (mass flux, fire area, wind speed<sup>-1</sup>, mixing depth<sup>-1</sup>), which  
359 gave monotonic increases for  $D_{pm}$ , show mixed results for  $\sigma$  due to variability in the initial  $\sigma_0$ . The time  
360 sensitivity plot (Fig. 8f) shows decreasing  $\sigma$  with time similar to Fig. 4b,d.

361 Emission  $\sigma_0$  shows the most pronounced and largest magnitude effect on output  $\sigma$  (~ -30% to  
362 +30%). Thus, the timescales for  $\sigma$  evolving towards 1.2 is longer than the timescales tested here for  
363 even the densest plumes. These sensitivity plots show that there is less variability in  $\sigma$  than in  $D_{pm}$  over  
364 the tested input space.

### 365 ***3.4 Simplified fits to the aged size distributions***

366 In addition to the GEM-SA emulator fits, we determined simplified fits for both  $D_{pm}$  and  $\sigma$  based on the  
367 behavior in Fig. 4 and Fig. 5. These fits are easier to implement in regional and global aerosol models  
368 than the full GEM-derived parameterization. These equations are meant to produce approximate  
369 estimates of  $D_{pm}$  and  $\sigma$  throughout plume size-distribution aging. The equations require: the initial  
370 value of the size-parameter of interest ( $D_{pm0}$  or  $\sigma_0$ ), a value proportional to the plume aerosol loading  
371 ( $dM/dxdz$ : mass flux · fire area / wind speed / mixing depth or  $dM/dx$ : mass flux · fire area / wind  
372 speed), and time since emission from the source fire (time). (Distance may also be used in these  
373 equations rather than time, and distance/wind-speed should be used in place of time.) The functional  
374 forms fitted for  $D_{pm}$  and  $\sigma$  are found below.

$$D_{pm} = D_{pm0} + A [dM/dx]^b (\text{time})^c \quad (1)$$

$$D_{pm} = D_{pm0} + A [dM/dxdz]^b (\text{time})^c \quad (2)$$

$$\sigma = \sigma_0 + A [dM/dx]^b (\text{time})^c (1.2 - \sigma_0) \quad (3)$$

$$\sigma = \sigma_0 + A [dM/dxdz]^b (\text{time})^c (1.2 - \sigma_0) \quad (4)$$

375

376 where A, b and c are determined by fitting each equation to the SAM-TOMAS data. For these  
377 empirical equations, the units of  $dM/dx$  are  $kg\ m^{-1}$ ,  $dM/dxdz$  are  $kg\ m^{-2}$ ,  $D_{pm}$  is nm and time since  
378 emission is min. It should be noted that the equations for  $D_{pm}$  and  $\sigma$  are designed to be independent of  
379 each other (i.e.  $D_{pm}$  is not dependent on  $\sigma_0$ ), which differs from the GEM-SA emulator. The aerosol  
380 loading parameter  $dM/dx$  was chosen based on the stratification seen in Fig. 4c and Fig. 5.  $dM/dxdz$   
381 was tested as well, as it incorporates the variance associated with mixing depth into the fit. The fit to  
382  $dM/dx$  rather than  $dM/dxdz$  may be advantageous because we expect mixing depth of the plume to be  
383 one of the more uncertain parameters in an atmospheric model, and the  $D_{pm}$  sensitivities to mixing  
384 depth tend to be smaller than those to mass flux, fire area and wind speed in the GEM-SA emulator  
385 (Fig. 7). The  $\sigma$  fits introduce a fourth factor,  $(1.2-\sigma_0)$ , which represents the difference between the  
386 SAM-TOMAS infinite-coagulation limit (Fig. 4b and d) and the initial modal width.

387 The scalar A, b and c variables were fit to the ensemble of SAM-TOMAS data. Their values are  
388 summarized in Table 3. The fits were tested against independent SAM-TOMAS data in Fig. 9 ( $D_{pm}$ ) and  
389 Fig. 10 ( $\sigma$ ). The simplified  $D_{pm}$  parameterizations, as expected, are not as good a fit of the SAM-  
390 TOMAS data as the GEM-SA emulator (Fig. 6). The fit statistics for the simple parameterizations are  
391 as follows:  $D_{pm}(dM/dx)$ : slope = 0.82,  $R^2 = 0.67$ , MNB= 0.003,  $D_{pm}(dM/dxdz)$ : slope = 0.98,  $R^2 = 0.77$ ,  
392 MNB= 0.008. The fit using  $dM/dxdz$  generally performs better than that with  $dM/dx$ . The simple  $\sigma$  fit  
393 also did not perform as well as the GEM-SA emulator with fit statistics of:  $\sigma(dM/dx)$ : slope = 0.64,  $R^2 =$   
394 0.78, MNB= 0.02 and,  $\sigma(dM/dxdz)$ : slope = 0.65,  $R^2 = 0.79$ , MNB= 0.01). Thus,  $dM/dxdz$  fits do yield  
395 better results than  $dM/dx$  (in particular for  $D_{pm}$ ); however, a user may choose to use the  $dM/dx$  fit if the  
396 mixing depth is unknown. We note that these fits are only valid within the parameter ranges shown in  
397 Table 1.  $dM/dV$  was also tested as a parameter within these simplified parameterization, but did not  
398 yield better agreements for either  $D_{pm}$  or  $\sigma$  than  $dM/dxdz$  despite incorporating an additional plume  
399 parameter (initial plume y-extent). This is because  $dM/dxdz$  is the product of  $dM/dV$  and the initial  
400 plume width; since wider plumes are less susceptible to dilution than narrower plumes,  $dM/dxdz$   
401 captures this plume-width effect while  $dM/dV$  does not.

### 402 **3.5 OA production/loss**

403 One of the limitations of the coagulation-only parameterizations derived in this paper is that they do not  
404 include the effects of potential condensation/evaporation of organic aerosol on the aged biomass-  
405 burning size distribution. Both condensational growth and evaporative loss of OA has been observed



406 previously in chamber studies and the field due to OA production or evaporation from  
 407 dilution/chemistry (Cubison et al., 2011; Hecobian et al., 2011; Hennigan et al., 2011; Grieshop et al.,  
 408 2009; Ortega et al., 2013; Jolleys et al., 2015; Vakkari et al., 2014). Konovalov et al. (2015) has  
 409 emphasized the importance of OA simulation in modeling long-range (>1000 km) plume evolution.  
 410 Thus, in order to predict biomass-burning aerosol mass, and thus the aerosol size distribution, we must  
 411 understand how OA evolves in biomass-burning plumes.

412 Here we present a simple correction to our coagulation-only parameterizations to account for  
 413 in-plume OA production/loss, assuming that this production/loss is known. This correction assumes all  
 414 SOA condenses onto existing particles (no new-particle formation). Each parameterization presented in  
 415 this paper may be corrected to include OA production/evaporation using the corrections below. We  
 416 assume that the OA production or loss does not affect the coagulation rates or  $\sigma$ , but acts to increase the  
 417 final  $D_{pm}$ . These assumptions are imperfect as irreversible condensation (evaporation) indecreases  
 418 (indecreases)  $\sigma$ ; however,  $\sigma$  is preserved during condensation or evaporation of semi-volatile material  
 419 (Pierce et al., 2011). Regardless, for the relatively small amounts of OA condensation/evaporation  
 420 considered here, the change in  $\sigma$  and coagulation rates should be minor. For a factor of 25% growth in  
 421 diameter from SOA, which may be expected from for a factor of 2 increase in OA mass with a small  
 422 change in sigma, we expect coagulation rates to stay within about 10% (Seinfeld and Pandis, 2006).  
 423 For larger changes in OA mass (more than a factor of  $\sim 2$ ) due to production/loss, our simple correction  
 424 will have uncertainties due to these assumptions. Our correction to the final  $D_{pm}$  has the following  
 425 form:

$$D_{pm\ w/OA\ prod/loss} = D_{pm\ w/o\ OA\ prod/loss} \cdot \left( \frac{OAMass_{w/OA\ prod/loss} + BCMass}{OAMass_{w/o\ OA\ prod/loss} + BCMass} \right)^{1/3} \quad (5)$$

426  
 427 where  $D_{pm\ w/o\ OA\ prod/loss}$  is the final  $D_{pm}$  from the coagulation-only GEM-SA emulator parameterization,  
 428 the biomass-burning aerosol OA mass (with and without additional production or loss) is in kg (per  
 429 particle or volume of air) and the BC mass is in kg (per particle or volume of air). Thus, for a doubling  
 430 of OA due to SOA production (one of the larger enhancements found in Hennigan et al., 2011),  
 431 particles that contain negligible BC will grow in diameter by 26% above the coagulation-only  
 432 predictions. If the particles contained 50% BC, then the diameter growth would only be 14%.

433 While these changes are expected to be on the large end for growth by SOA production, they

434 are significantly smaller than the ~200% variability in aged  $D_{pm}$  due to coagulation over the range of  
435 initial fire conditions (Fig. 7). For example, variations in wind speed, mass flux, and fire area alone can  
436 independently cause variability in the aged  $D_{pm}$  by a factor of 2 due to changes in coagulation rates  
437 while variability in condensational growth appears to cause much smaller uncertainties (~25%) in the  
438 aged  $D_{pm}$ . This indicates that although SOA condensational growth is certainly important in shaping  
439 particle composition and total particle mass, it is not among the most dominant factors determining the  
440 aged  $D_{pm}$  compared to those fire-condition parameters controlling coagulation growth. It should be  
441 noted, however, that the  $D_{pm}$  growth attributed to OA condensation is not accompanied by a change in  
442 particle number (additional OA mass is distributed among existing particles), whereas a similar  
443 increase in  $D_{pm}$  growth by coagulation only would have an accompanying decrease in particle number.  
444 Thus, the [changes to the aerosol size distribution and](#) climatic influence of a size change due to  
445 coagulation and condensation are different.

### 446 *3.6 Estimating aged size distributions observed at the Mt. Bachelor Observatory*

447 The simplified fits presented in Section 3.4 (equations 1-4) were tested against size distributions  
448 measurements of biomass-burning plumes observed at the Mt. Bachelor Observatory (MBO) in Central  
449 Oregon (43.98°N, 121.69°W, 2,764 m a.s.l.). MBO is a mountaintop site that has been in operation  
450 since 2004 (Jaffe et al., 2005). An intensive campaign was performed during the summer of 2015 to  
451 measure aerosol physical and optical properties of wildfire emissions (Laing et al., in prep). During this  
452 campaign aerosol size distributions from 14.1 to 637.8 nm were measured with a Scanning Mobility  
453 Particle Sizer (SMPS). Additional details about MBO and the sampling campaign can be found in  
454 Laing et al. (in prep).

455 We identified eleven biomass-burning plumes during August (Table 4). Criteria for plume  
456 selection was aerosol scattering  $> 20 \text{ Mm}^{-1}$  and CO  $> 150 \text{ ppbv}$  for at least an hour, a strong correlation  
457 ( $R^2 > 0.80$ ) between aerosol scattering and CO, and consistent backward trajectories indicating  
458 transport over known fire locations. We calculated back-trajectories to determine fire locations using  
459 the National Oceanic and Atmospheric Administration Hybrid Single-Particle Lagrangian Integrated  
460 Trajectory (HYSPLIT) model, version 4 (Draxler, 1999; Draxler and Hess, 1997, 1998; Stein et al.,  
461 2015) with Global Data Assimilation System (GDAS,  $1^\circ \times 1^\circ$ ) data. The Mt. Bachelor summit is located  
462 at ~1500 m amgl (above model ground level), so the back-trajectory starting heights of 1300, 1500, and  
463 1700 m amgl were chosen (Ambrose et al., 2011). Fire locations were identified using Moderate

464 [Resolution Imaging Spectroradiometer \(MODIS\) satellite-derived active fire counts](#)  
465 (<http://activefiremaps.fs.fed.us/>; Justice et al., 2002).

466 [For the plume aerosol loading parameterization inputs in equations 1-4, we used Fire INventory](#)  
467 [from NCAR \(FINN\) daily-averaged fire area and fire-emissions estimates \(Wiedinmyer et al. 2011\).](#)  
468 [Multiple FINN data points in the same vicinity were combined based on the location of large-wildfire](#)  
469 [incidents tracked by the National Interagency Fire Center \(NIFC\) \(<http://activefiremaps.fs.fed.us/>\).](#) We  
470 [calculated the mass flux for the aerosol-loading estimates \( \$dM/dxdz\$  and  \$dM/dx\$ \) using these FINN](#)  
471 [OC+BC emissions \(kg/day\) and FINN fire area data \( \$km^2\$ \). Mixing depth was defined as the mixing](#)  
472 [depth at the source location of the fire in the Global Data Assimilation System \(GDAS,  \$1^\circ \times 1^\circ\$ \) data.](#)  
473 [Wind speed was also extracted from GDAS data and was calculated as the average wind speed from the](#)  
474 [ground to the defined mixing height. If no data were available, the mixing height and wind speed were](#)  
475 [set to 660 m and 8.5 m/s based on the median value of the rest of the plumes. We assumed the emission](#)  
476 [diameter \( \$D\_{pm0}\$ \) to be 100 nm, and we calculated  \$\sigma\$  using initial modal widths \( \$\sigma\_0\$ \) of 1.6, 1.9 and 2.4, to](#)  
477 [be discussed later. We estimated the transport time from plume back-trajectories, and these values](#)  
478 [ranged from 4.5 to 35 hours.](#)

479 [The measured and calculated size distribution diameter and modal widths for each plume at](#)  
480 [MBO are summarized in Table 4. We calculated  \$D\_{pm}\$  and  \$\sigma\$  as the geometric mean diameter and](#)  
481 [geometric standard deviation of the plume averaged size distribution \[as measured by the SMPS\]\(#\),](#)  
482 [respectively. The plume-averaged size distributions may be influenced by non-biomass-burning](#)  
483 [particles included along the trajectory from the wildfire. Plumes 1, 2, and 4 have bimodal distributions.](#)  
484 [The second mode \(Aitken mode\) of these distributions are an example of influence from a non-biomass](#)  
485 [burning source. These three bimodal distributions have inflated  \$\sigma\$  values, which will be addressed later.](#)  
486 [Due to the large number of fires in Northern California and Oregon during the summer of 2015, some](#)  
487 [of the plumes observed at MBO were influenced by more than one fire \(e.g. Figure 9\). For these](#)  
488 [plumes, we calculated aged  \$D\_{pm}\$  and  \$\sigma\$  values for each fire area \(black squares in Figure 9\) and a](#)  
489 [weighted average based on aerosol loading \( \$dM/dx\$  or  \$dM/dxdz\$ \) was taken. Column 3 in Table 4](#)  
490 [indicates how many fire areas were averaged for each plume.](#)

491 [Figure 10 shows the predicted aged  \$D\_{pm}\$  plotted against the observed values for both the  \$dM/dx\$](#)   
492 [and  \$dM/dxdz\$  forms of the simple parameterization. An initial  \$D\_{pm0}\$  of 100 nm was assumed.](#)  
493 [used Equation 2 \(using aerosol mass loading  \$dM/dxdz\$ \) estimates  \$D\_{pm}\$  somewhat more accurately \( \$y =\$](#)   
494 [0.93x + 17.1,  \$R^2 = 0.551\$ \) than Eqn. 1, which uses aerosol mass loading  \$dM/dx\$  \( \$y = 0.62x + 53.1\$ ,  \$R^2 =\$](#)

495 0.532). Over half of the variability in the observed  $D_{pm}$  was captured by the simplified fits. Thus, the  
496 simple parameterizations show skill at predicting the aged  $D_{pm}$  values relative to choosing a constant  
497 value of aged  $D_{pm}$  as is typically done in regional and global models.

498 Figure 11 shows the predicted aged  $\sigma$  plotted against the observed values for both  
499 parameterization forms. Both parameterizations do not predict modal width as well as  $D_{pm}$  (Figure 11).  
500 The calculated modal width changed significantly when using different emission modal-width values  
501 ( $\sigma_0$ ). Janhäll et al. (2010) found the  $\sigma$  of fresh biomass burning emissions to range from  $\sim 1.6$  to  $1.9$ .  
502 When using a  $\sigma_0$  of  $1.6$ , we underestimated all of the  $\sigma$  values. Using a  $\sigma_0$  of  $1.9$ , we improved the  
503 estimation of aged  $\sigma$  ranging from  $1.4$ - $1.6$  (Figure 11a). The three higher measured  $\sigma$  values are from  
504 the bimodal plumes mentioned previously, which have larger  $\sigma$  values than would be due strictly to the  
505 biomass-burning plume. We found that using a  $\sigma_0$  of  $2.4$  provided the best fit for all of the measured  
506 plumes (Figure 11b),  $2.4$  being the max  $\sigma_0$  value from Table 2. The  $\sigma$  simplified fits using  $\sigma_0 = 2.4$  have  
507 statistics of:  $\sigma(dM/dx): y = 0.50 + 1.00, R^2 = 0.513$ , and  $\sigma(dM/dxdz): y = 0.57 + 0.77, R^2 = 0.468$ .  
508 Thus, both parameterizations do not predict modal width as well as  $D_{pm}$ ; however, these  
509 parameterizations do show skill relative to assuming a constant value of  $\sigma$ .

510 The results from the regional fires demonstrate that the parameterizations in Eqs 1-4 can be  
511 successfully used to estimate aged biomass-burning size distributions in regional biomass-burning  
512 plumes with transport times up to 35 hours with significantly better skill than assuming fixed values for  
513 size-distribution parameters. More investigations of individual aged biomass-burning plumes,  
514 specifically with one clear source, should be completed to fully characterize this parameterization.

515 |

## 516 **4. Conclusions**

517 We used the SAM-TOMAS large-eddy simulation model and an emulation technique to explore the  
518 evolution of biomass-burning aerosol size distributions due to coagulation and build coagulation-only  
519 parameterizations of this size-distribution evolution. We have also provided a simple correction to the  
520 parameterization for cases with net OA production or loss. We used the SAM-TOMAS model to  
521 simulate plume dispersion and aerosol coagulation. The SAM-TOMAS results show that the aged  $D_{pm}$   
522 can be largely described by  $dM/dx$  and the distance from the source (or time since emission). These

523 results also show that the aged  $\sigma$  moves from  $\sigma_0$  towards a value of 1.2 at a rate that depends on  $dM/dx$ .

524 The GEM-SA program was used to derive a  $D_{pm}$  and  $\sigma$  emulator parameterization based on the  
525 SAM-TOMAS results. The parameterization requires seven input parameters: emission  $D_{pm0}$ , emission  
526  $\sigma_0$ , mass flux, boundary layer wind speed, fire area, plume mixing depth, and time since emission. The  
527 predicted  $D_{pm}$  and  $\sigma$  can then be used as effective unimodal biomass-burning size-distribution  
528 parameters in regional and global aerosol models.

529 The  $D_{pm}$  parameterization showed the strongest sensitivities to those input parameters associated  
530 with the extent of aerosol loading within the plume (mass flux, fire area, wind speed). Across the fire  
531 area and wind speed ranges tested here, final  $D_{pm}$  varied by  $\pm 50\%$ . Mass flux had the largest associated  
532  $D_{pm}$  sensitivity across the tested values (-50% to +100%). These sensitivities were larger than those  
533 associated with mixing depth ( $\sim -20\%$  to  $20\%$ ) or the initial size-distribution parameters ( $D_{pm0}$ :  $\sim -25\%$   
534 to  $25\%$ ,  $\sigma_0$ :  $\sim 15\%$  to  $-15\%$ ). The  $\sigma$  parameterization showed a uniform decrease in  $\sigma$  with time and  
535 strong sensitivities to the emission  $\sigma_0$  (-30% to 30%). This strong sensitivity to  $\sigma_0$  can be attributed to  
536 the inertia in  $\sigma$  evolution in simulations with large modal widths and relatively small mass loading,  
537 where  $\sigma$  will not converge quickly to the coagulation limit (1.2).

538 The GEM-SA-derived parameterization performed relatively well against the SAM-TOMAS  
539 model with a correlation of  $R^2=0.83$ , slope of  $m=0.92$  and a low mean normalized bias of  $MNB=-0.06$   
540 for  $D_{pm}$ . The  $\sigma$  parameterization has fit statistics of  $R^2= 0.93$ , slope= 0.91 and  $MNB= 0.01$ . The  $\sigma$   
541 parameterization was unable to capture the coagulation limit of 1.2 seen in the SAM-TOMAS results  
542 and instead extrapolated to lower values. This 1.2 limit differs from the 1.32  $\sigma$  limit proposed by Lee  
543 (1983) due to the bin-spacing in SAM-TOMAS being coarser than lognormal modes with these small  
544 modal widths.

545 We also provided simplified polynomial fits for  $D_{pm}$  and  $\sigma$  (Eqns 1-4, Table 3) for calculating  
546 aged  $D_{pm}$  and  $\sigma$  as independent functions of: the fresh emission parameter ( $D_{pm0}$  or  $\sigma_0$ ), the mass loading  
547 of the aerosol ( $dM/dx$  or  $dM/dxdz$ ) and the time since emission from the source fire. The  $\sigma$  fits also  
548 require a convergence term to account for the coagulation limit (1.2 in the SAM-TOMAS model).  
549 Tested against independent SAM-TOMAS data, the  $D_{pm}$  simplified fits performed as:  $D_{pm}(dM/dx)$ :  
550 slope = 0.82,  $R^2 = 0.67$ ,  $MNB= 0.003$  and  $D_{pm}(dM/dxdz)$ : slope = 0.98,  $R^2 = 0.77$ ,  $MNB= 0.008$ . The  $\sigma$   
551 simplified fits have statistics of  $\sigma(dM/dx)$ : slope = 0.64,  $R^2= 0.78$ ,  $MNB= 0.02$  and  $\sigma(dM/dxdz)$ : slope  
552 = 0.65,  $R^2 = 0.79$ ,  $MNB= 0.01$ . The equations requiring  $(dM/dxdz)$  performed better than their  $(dM/dx)$

553 counterparts as they also account for the aerosol layer depth.

554 We provided a correction for OA production/loss, and showed that significant production of  
555 SOA within the plume (~ 100% OA mass enhancement) would cause a relatively small shift in the size-  
556 distribution  $D_{pm}$  (14-26% increase) compared to other factors that control the coagulation rate (e.g.  
557  $dM/dx$ ). We note, however, that OA production increases  $D_{pm}$  without loss of particle number while  
558 coagulation increases  $D_{pm}$  with a decrease in number, thus the climatic impact of condensation and  
559 coagulation are different. The simplified OA-production/loss correction assumes no change in  $\sigma$  with  
560 condensational growth. Further testing should be done with explicit OA production and loss to better  
561 quantify the effects of condensation of the size-distribution evolution.

562 We tested the simplified fits for  $D_{pm}$  and  $\sigma$  (Eqns 1-4, Table 3) against 11 aged biomass-burning  
563 plumes observed at the Mt. Bachelor Observatory in August of 2015.  $D_{pm}$  was reasonably calculated  
564 using both measures of aerosol loading,  $dM/dx$  and  $dM/dxdz$  ( $R^2$  values above 0.7 without an outlier).  
565 The fit of calculated  $\sigma$  and measured  $\sigma$  depended heavily on the assumed initial modal width, with an  
566 assumed  $\sigma_0$  of 2.4 working best in our case ( $R^2$  values around 0.75 without an outlier). Despite the  
567 changes in calculated  $D_{pm}$  and  $\sigma$  due to the estimated emission size distribution, the parameterizations  
568 captured the differences from plume to plume in regional biomass-burning plumes, which is based on  
569 estimated aerosol loading and transport times.

570 Our analysis does not include any cloud processing of the plume particles, i.e. the production of  
571 aqueous SOA within activated plume particles is not accounted for in our simple OA mass correction.  
572 The production of SOA within droplets could result in additional SOA mass being only added to the  
573 larger, activated particles during activation/evaporation cycling. This extra SOA mass would favor  
574 increases in the diameters of the larger particles of the size-distribution only, which could create a  
575 bimodal size distribution and increase the overall coagulation rates in the plume (more, larger  
576 particles coagulate more rapidly with the small-diameter particles).

577 Future work includes (1) more testing of the parameterizations developed in this work against  
578 real world observations of size distribution aging, and (2) incorporating the parameterizations into  
579 regional and global aerosol models for further evaluation against regional/global measurements.

580

## 581 **5. Author Contribution**

582 K.M. Sakamoto, R.G. Stevens, and J.R. Pierce designed the study. K. M. Sakamoto performed the  
583 SAM-TOMAS simulations, and created and evaluated the parameterizations. [J.R. Laing tested the](#)  
584 [parameterizations size distributions of aged biomass burning plumes observed at the Mt. Bachelor](#)  
585 [Observatory, and D.A. Jaffe oversaw the Mt. Bachelor measurements.](#) K. M. Sakamoto prepared the  
586 manuscript with assistance from all co-authors.

## 587 **6. Acknowledgements**

588 NCEP Reanalysis data provided by the NOAA/OAR/ESRL PSD, Boulder, Colorado, USA, from their  
589 Web site at <http://www.esrl.noaa.gov/psd/>. K.M. Sakamoto was funded by a [Natural Sciences and](#)  
590 [Engineering Research Council of Canada](#) (NSERC) PGS-M Fellowship. [The authors gratefully](#)  
591 [acknowledge the NOAA Air Resources Laboratory \(ARL\) for the provision of the HYSPLIT transport](#)  
592 [model used in this publication](#)

593

## 594 **7. References**

- 595 Adams, P. J. and Seinfeld, J. H.: Predicting global aerosol size distributions in general circulation  
596 models, *Journal of Geophysical Research-Atmospheres*, 107, 4310 - 4370, 2002.
- 597 Adler, G., Flores, J. M., Abo Riziq, A., Borrmann, S. and Rudich, Y.: Chemical, physical, and optical  
598 evolution of biomass burning aerosols: a case study, *Atmos. Chem. Phys.*, 11(4), 1491–1503,  
599 doi:10.5194/acp-11-1491-2011, 2011.
- 600 [Akagi, S. K., Craven, J. S., Taylor, J. W., McMeeking, G. R., Yokelson, R. J., Burling, I. R., Urbanski,](#)  
601 [S. P., Wold, C. E., Seinfeld, J. H., Coe, H., Alvarado, M. J. and Weise, D. R.: Evolution of trace](#)  
602 [gases and particles emitted by a chaparral fire in California, \*Atmos. Chem. Phys.\*, 12\(3\), 1397–](#)  
603 [1421, doi:10.5194/acp-12-1397-2012, 2012.](#)
- 604 Alonso-Blanco, E., Calvo, A. I., Pont, V., Mallet, M., Fraile, R. and Castro, A. Impact of Biomass  
605 Burning on Aerosol Size Distribution, Aerosol Optical Properties and Associated Radiative  
606 Forcing, *Aerosol Air Qual. Res.*, 006, 708–724, doi:10.4209/aaqr.2013.05.0163, 2014.
- 607 [Ambrose, J.L., Reidmiller, D.R. and Jaffe, D.A.: Causes of High O3 in the Lower Free Troposphere](#)  
608 [over the Pacific Northwest as Observed at the Mt. Bachelor Observatory. \*Atmos. Environ.\*, 45,](#)  
609 [5302–5315, 2011.](#)
- 610 Andreae, M. O. and Merlet, P.: Emission of trace gases and aerosols from biomass burning, *Global*  
611 *Biogeochem. Cycles*, 15(4), 955–966, doi:10.1029/2000GB001382, 2001.
- 612 Boucher, O., Randall, D., Artaxo, P., Bretherton, C., Feingold, G., Forster, P., Kerminen, V.-M., Kondo,



- 613 Y., Liao, H., Lohmann, U., Rasch, P., Satheesh, S. K., Sherwood, S., Stevens, B. & Zhang, X. Y.  
614 in *Climate Change 2013: The Physical Science Basis. Contribution of Working Group I to the*  
615 *Fifth Assessment Report of the Intergovernmental Panel on Climate Change* (eds. Stocker, T. F.  
616 et al.) (Cambridge University Press, 2013).
- 617 Capes, G., Johnson, B., McFiggans, G., Williams, P. I., Haywood, J., and Coe, H.: Aging of biomass  
618 burning aerosols over West Africa: Aircraft measurements of chemical composition, microphysical  
619 properties, and emission ratios, *Journal of Geophysical Research*, 113, D00C15,  
620 doi:10.1029/2008JD009845, 2008.
- 621 Carrico, C. M., Petters, M. D., Kreidenweis, S. M., Sullivan, A. P., McMeeking, G. R., Levin, E. J. T.,  
622 Engling, G., Malm, W. C. and Collett, J. L.: Water uptake and chemical composition of fresh  
623 aerosols generated in open burning of biomass, *Atmos. Chem. Phys.*, 10(11), 5165–5178,  
624 doi:10.5194/acp-10-5165-2010, 2010.
- 625 Carslaw, K. S., Lee, L. A., Reddington, C. L., Pringle, K. J., Rap, A., Forster, P. M., Mann, G. W.,  
626 Spracklen, D. V, Woodhouse, M. T., Regayre, L. A. and Pierce, J. R.: Large contribution of natural  
627 aerosols to uncertainty in indirect forcing, *Nature*, 503(7474), 67–71 doi:10.1038/nature12674,  
628 2013.
- 629 Cubison, M. J., Ortega, a. M., Hayes, P. L., Farmer, D. K., Day, D., Lechner, M. J., Brune, W. H., Apel,  
630 E., Diskin, G. S., Fisher, J. a., Fuelberg, H. E., Hecobian, a., Knapp, D. J., Mikoviny, T., Riemer,  
631 D., Sachse, G. W., Sessions, W., Weber, R. J., Weinheimer, A. J., Wisthaler, a., and Jimenez, J. L.:  
632 Effects of aging on organic aerosol from open biomass burning smoke in aircraft and laboratory  
633 studies, *Atmospheric Chemistry and Physics*, 11, 12 049-12 064, doi:10.5194/acp-11-12049-2011,  
634 2011.
- 635 DeCarlo, P. F., Ulbrich, I. M., Crouse, J., de Foy, B., Dunlea, E. J., Aiken, A. C., Knapp, D.,  
636 Weinheimer, A. J., Campos, T., Wennberg, P. O. and Jimenez, J. L.: Investigation of the sources  
637 and processing of organic aerosol over the Central Mexican Plateau from aircraft measurements  
638 during MILAGRO, *Atmos. Chem. Phys.*, 10(12), 5257–5280, doi:10.5194/acp-10-5257-2010,  
639 2010.
- 640 [Draxler, R.R.: HYSPLIT\\_4 User's Guide, NOAA Technical Memorandum ERL ARL-230, June, 35 pp.,](#)  
641 [1999.](#)
- 642 [Draxler, R.R., and Hess, G.D.: An overview of the HYSPLIT\\_4 modelling system for trajectories,](#)  
643 [dispersion, and deposition. \*Australian Meteorological Magazine\*, 47: 295-308, 1998.](#)
- 644 [Draxler, R.R., and Hess, G.D.: Description of the HYSPLIT\\_4 modeling system. NOAA Technical](#)  
645 [Memo ERL ARL-224, December, 24 p., 1997.](#)
- 646 Engelhart, G. J., Hennigan, C. J., Miracolo, M. A., Robinson, A. L. and Pandis, S. N.: Cloud  
647 condensation nuclei activity of fresh primary and aged biomass burning aerosol, *Atmos. Chem.*  
648 *Phys.*, 12(15), 7285–7293, doi:10.5194/acp-12-7285-2012, 2012.
- 649 Freitas, S. R., Longo, K. M., Chatfield, R., Latham, D., Dias, M. A. F. S., Andreae, M. O., Prins, E.,  
650 and Unesp, F. E. G.: Including the sub-grid scale plume rise of vegetation fires in low resolution  
651 atmospheric transport models, *Atmospheric Chemistry and Physics*, pp. 3385 - 3398, 2007.
- 652 Grieshop, A. P., Logue, J. M., Donahue, N. M. and Robinson, A. L.: Laboratory investigation of  
653 photochemical oxidation of organic aerosol from wood fires 1: measurement and simulation of  
654 organic aerosol evolution, *Atmos. Chem. Phys.*, 9(4), 1263–1277, doi:10.5194/acp-9-1263-2009,  
655 2009.



- 656 Haywood, J. and Boucher, O.: Estimates of the direct and indirect radiative forcing due to tropospheric  
657 aerosols: a review, *Rev. Geophys.*, 38, 513–543, doi:10.1029/1999RG000078, 2000.
- 658 Hecobian, A., Liu, Z., Hennigan, C. J., Huey, L. G., Jimenez, J. L., Cubison, M. J., Vay, S., Diskin, G.  
659 S., Sachse, G. W., Wisthaler, A., Mikoviny, T., Weinheimer, A. J., Liao, J., Knapp, D. J.,  
660 Wennberg, P. O., Kürten, A., Crounse, J. D., Clair, J. St., Wang, Y. and Weber, R. J.: Comparison  
661 of chemical characteristics of 495 biomass burning plumes intercepted by the NASA DC-8 aircraft  
662 during the ARCTAS/CARB-2008 field campaign, *Atmos. Chem. Phys.*, 11(24), 13325–13337,  
663 doi:10.5194/acp-11-13325-2011, 2011.
- 664 Hennigan, C. J., Miracolo, M. A., Engelhart, G. J., May, A. A., Presto, A. A., Lee, T., Sullivan, A. P.,  
665 McMeeking, G. R., Coe, H., Wold, C. E., Hao, W.-M., Gilman, J. B., Kuster, W. C., de Gouw, J.,  
666 Schichtel, B. A., Kreidenweis, S. M. and Robinson, A. L.: Chemical and physical transformations  
667 of organic aerosol from the photo-oxidation of open biomass burning emissions in an  
668 environmental chamber, *Atmos. Chem. Phys.*, 11(15), 7669–7686, doi:10.5194/acp-11-7669-2011,  
669 2011.
- 670 Hennigan, C. J., Westervelt, D. M., Riipinen, I., Engelhart, G. J., Lee, T., Collett, J. L., Pandis, S. N.,  
671 Adams, P. J. and Robinson, A. L.: New particle formation and growth in biomass burning plumes:  
672 An important source of cloud condensation nuclei, *Geophys. Res. Lett.*, 39(9), n/a–n/a,  
673 doi:10.1029/2012GL050930, 2012.
- 674 Heringa, M. F., DeCarlo, P. F., Chirico, R., Tritscher, T., Dommen, J., Weingartner, E., Richter, R.,  
675 Wehrle, G., Prévôt, A. S. H. and Baltensperger, U.: Investigations of primary and secondary  
676 particulate matter of different wood combustion appliances with a high-resolution time-of-flight  
677 aerosol mass spectrometer, *Atmos. Chem. Phys.*, 11(12), 5945–5957, doi:10.5194/acp-11-5945-  
678 2011, 2011.
- 679 Hobbs, P. V., Sinha, P., Yokelson, R. J., Christian, T. J., Blake, D. R., Gao, S., Kirchstetter, T. W.,  
680 Novakov, T. and Pilewskie, P.: Evolution of gases and particles from a savanna fire in South  
681 Africa, *J. Geophys. Res.*, 108(D13), doi:10.1029/2002JD002352, 2003.
- 682 Hosseini, S., Li, Q., Cocker, D., Weise, D., Miller, A., Shrivastava, M., Miller, J. W., Mahalingam, S.,  
683 Princevac, M. and Jung, H.: Particle size distributions from laboratory-scale biomass fires using  
684 fast response instruments, *Atmos. Chem. Phys.*, 10(16), 8065–8076, doi:10.5194/acp-10-8065-  
685 2010, 2010.
- 686 Huffman, J. A., Docherty, K. S., Mohr, C., Cubison, M. J., Ulbrich, I. M., Ziemann, P. J., Onasch, T. B.  
687 and Jimenez, J. L.: Chemically-Resolved Volatility Measurements of Organic Aerosol from  
688 Different Sources, *Environ. Sci. Technol.*, 43(14), 5351–5357, doi:10.1021/es803539d, 2009.
- 689 Jacobson, M. Z.: Strong radiative heating due to the mixing state of black carbon in atmospheric  
690 aerosols, *Nature*, 409(6821), 695–697, 2001.
- 691 [Jaffe, D., Prestbo, E., Swartzendruber, P., Weisspenzias, P., Kato, S., Takami, a, Hatakeyama, S. and](#)  
692 [Kajii, Y.: Export of atmospheric mercury from Asia, \*Atmos. Environ.\*, 39\(17\), 3029–3038,](#)  
693 [doi:10.1016/j.atmosenv.2005.01.030, 2005.](#)
- 694 Janhäll, S., Andreae, M. O. and Pöschl, U.: Biomass burning aerosol emissions from vegetation fires :  
695 particle number and mass emission factors and size distributions, *Atmos. Chem. Phys.*, 1427–1439,  
696 2010.
- 697 [Jolleys, M. D., Coe, H., Mcfiggans, G., Taylor, J. W., Shea, S. J. O., Breton, M. Le, Bauguitte, S. J.,](#)  
698 [Moller, S., Carlo, P. Di, Aruffo, E., Palmer, P. I., Lee, J. D., Percival, C. J. and Gallagher, M. W.:](#)

699 | [Properties and evolution of biomass burning organic aerosol from Canadian boreal forest fires, ,](#)  
700 | [3077–3095, doi:10.5194/acp-15-3077-2015, 2015.](#)

701 | [Justice, C. , Giglio, L., Korontzi, S., Owens, J., Morissette, J. , Roy, D., Descloitres, J., Alleaume, S.,](#)  
702 | [Petitcolin, F. and Kaufman, Y.: The MODIS fire products, Remote Sens. Environ., 83\(1-2\), 244–](#)  
703 | [262, doi:10.1016/S0034-4257\(02\)00076-7, 2002.](#)

704 | Kennedy, M. and O'Hagan, A.: Bayesian calibration of computer models, J. R. Stat. Soc. Ser. B Stat.  
705 | Methodol., 63, 425 - 464, 2001.

706 | Kennedy, M., Anderson, C., O'Hagan, A., Lomas, M., Woodward, I., Gosling, J. P., and Heinemeyer, A.:  
707 | Quantifying uncertainty in the biospheric carbon flux for England and Wales, Journal of the Royal  
708 | Statistical Society: Series A (Statistics in Society), 171, 109-135, doi:10.1111/j.1467-  
709 | 985X.2007.00489.x, 2008.

710 | Khairoutdinov, M. F. and Randall, D. A.: Cloud resolving modeling of the ARM summer 1997 IOP:  
711 | Model formulation, results, uncertainties, and sensitivities, Journal of the Atmospheric Sciences,  
712 | 60, 607-625, 2003.

713 | [Konovalov, I. B., Beekmann, M., Berezin, E. V, Petetin, H., Mielonen, T., Kuznetsova, I. N. and](#)  
714 | [Andreae, M. O.: The role of semi-volatile organic compounds in the mesoscale evolution of](#)  
715 | [biomass burning aerosol : a modeling case study of the 2010 mega-fire event in Russia, , 13269–](#)  
716 | [13297, doi:10.5194/acp-15-13269-2015, 2015.](#)

717 | [Laing, J.R., J. Hee, and D.A. Jaffe. Physical and Optical Properties of Aged Biomass Burning Aerosol](#)  
718 | [during an Exceptional Forest Fire Year in the Pacific Northwest. In Preparation.](#)

719 | Lee, K.: Change of particle size distribution during Brownian coagulation, Journal of Colloid and  
720 | Interface Science, 92, 315 - 325, doi:http://dx.doi.org/10.1016/0021-9797(83)90153-4, 1983.

721 | Lee, L. A., Carslaw, K. S., Pringle, K. J., Mann, G. W., and Spracklen, D. V.: Emulation of a complex  
722 | global aerosol model to quantify sensitivity to uncertain parameters, Atmospheric Chemistry and  
723 | Physics, 11, 12 253{12 273, doi:10.5194/acp-11-12253-2011, 2011.

724 | Lee, L. A., Carslaw, K. S., Pringle, K. J., and Mann, G. W.: Mapping the uncertainty in global CCN  
725 | using emulation, Atmospheric Chemistry and Physics, 12, 9739 – 9751, doi:10.5194/acp-12-9739-  
726 | 2012, 2012.

727 | Lee, L. A., Pringle, K. J., Reddington, C. L., Mann, G. W., Stier, P., Spracklen, D. V., Pierce, J. R., and  
728 | Carslaw, K. S.: The magnitude and causes of uncertainty in global model simulations of cloud  
729 | condensation nuclei, Atmospheric Chemistry and Physics, 13, 8879-8914, doi:10.5194/acp-13-  
730 | 8879-2013, 2013.

731 | Levin, E. J. T., McMeeking, G. R., Carrico, C. M., Mack, L. E., Kreidenweis, S. M., Wold, C. E.,  
732 | Moosmüller, H., Arnott, W. P., Hao, W. M., Collett, J. L. and Malm, W. C.: Biomass burning  
733 | smoke aerosol properties measured during Fire Laboratory at Missoula Experiments (FLAME), J.  
734 | Geophys. Res., 115(D18), D18210, doi:10.1029/2009JD013601, 2010.

735 | Lonsdale, C. R., Stevens, R. G., Brock, C. a., Makar, P. a., Knipping, E. M., and Pierce, J. R.: The  
736 | effect of coal-powered power-plant SO<sub>2</sub> and NO<sub>x</sub> control technologies on aerosol nucleation in the  
737 | source plumes, Atmospheric Chemistry and Physics, 12, 11 519-11 531, doi:10.5194/acp-12-  
738 | 11519-2012, 2012.

739 | May, A. A., Levin, E. J. T., Hennigan, C. J., Riipinen, I., Lee, T., Collett, J. L., Jimenez, J. L.,  
740 | Kreidenweis, S. M. and Robinson, A. L.: Gas-particle partitioning of primary organic aerosol  
741 | emissions: 3. Biomass burning, J. Geophys. Res. Atmos., 118(19), 11,327–11,338,

742 | doi:10.1002/jgrd.50828, 2013.

743 | [May, A. A., Lee, T., Mcmeeking, G. R., Akagi, S., Sullivan, A. P., Urbanski, S. and Yokelson, R. J.:](#)  
744 | [Observations and analysis of organic aerosol evolution in some, , 6323–6335, doi:10.5194/acp-15-](#)  
745 | [6323-2015, 2015.](#)

746 | Mesinger, F., Dimego, G., Kalnay, E., Mitchell, K., Shafran, P. C., Ebisuzaki, W., Joviæ, D., Woollen,  
747 | J., Rogers, E., Berbery, E. H., Ek, M. B., Fan, Y., Grumbine, R., Higgins, W., Li, H., Lin, Y.,  
748 | Manikin, G., Parrish, D., and Shi, W.: North American Regional Reanalysis: A long-term,  
749 | consistent, high-resolution climate dataset for the North American domain, as a major  
750 | improvement upon the earlier global reanalysis datasets in both resolution and accuracy, *B. Am.*  
751 | *Meteorol. Soc.*, 87, 343–360, 2006.

752 | Okoshi, R., Rasheed, A., Chen Reddy, G., McCrowey, C. J. and Curtis, D. B.: Size and mass  
753 | distributions of ground-level sub-micrometer biomass burning aerosol from small wildfires,  
754 | *Atmos. Environ.*, 89, 392–402, doi:10.1016/j.atmosenv.2014.01.024, 2014.

755 | Ortega, A. M., Day, D. A., Cubison, M. J., Brune, W. H., Bon, D., de Gouw, J. A. and Jimenez, J. L.:  
756 | Secondary organic aerosol formation and primary organic aerosol oxidation from biomass-burning  
757 | smoke in a flow reactor during FLAME-3, *Atmos. Chem. Phys.*, 13(22), 11551–11571,  
758 | doi:10.5194/acp-13-11551-2013, 2013.

759 | Petters, M. D. and Kreidenweis, S. M.: A single parameter representation of hygroscopic growth and  
760 | cloud condensation nucleus activity, *Atmos. Chem. Phys.*, 7(8), 1961–1971, doi:10.5194/acp-7-  
761 | 1961-2007, 2007.

762 | Petters, M. D., Carrico, C. M., Kreidenweis, S. M., Prenni, A. J., DeMott, P. J., Collett, J. L. and  
763 | Moosmüller, H.: Cloud condensation nucleation activity of biomass burning aerosol, *J. Geophys.*  
764 | *Res.*, 114(D22), D22205, doi:10.1029/2009JD012353, 2009.

765 | Pierce, J. R., Chen, K. and Adams, P. J.: Contribution of primary carbonaceous aerosol to cloud  
766 | condensation nuclei: processes and uncertainties evaluated with a global aerosol microphysics  
767 | model, *Atmos. Chem. Phys.*, 7, 5447–5466, 2007.

768 | Pierce, J.R., Riipinen, I., Kulmala, M., Ehn, Petaja, T., Junninen, H., Worsnop, D.R., Donahue, N.M.:  
769 | Quantification of the volatility of secondary organic compounds in ultrafine particles during  
770 | nucleation events, *Atmospheric Chemistry and Physics*, 11, 9019-9036, doi:10.5194/acp-11-9019-  
771 | 2011, 2011.

772 | Reid, J. S., Koppmann, R., Eck, T. F. and Eleuterio, D. P.: A review of biomass burning emissions part  
773 | II: intensive physical properties of biomass burning particles, *Atmos. Chem. Phys.*, 5(3), 799–825,  
774 | doi:10.5194/acp-5-799-2005, 2005.

775 | Rissler, J., Vestin, A., Swietlicki, E., Fisch, G., Zhou, J., Artaxo, P. and Andreae, M. O.: Size  
776 | distribution and hygroscopic properties of aerosol particles from dry-season biomass burning in  
777 | Amazonia, *Atmos. Chem. Phys.*, 6, 471–491, 2006.

778 | Sakamoto, K. M., Allan, J. D., Coe, H., Taylor, J. W., Duck, T. J., and Pierce, J. R.: Aged boreal  
779 | biomass-burning aerosol size distributions from BORTAS 2011, *Atmos. Chem. Phys.*, 15, 1633-  
780 | 1646, doi:10.5194/acp-15-1633-2015, 2015.

781 | Seinfeld, J. H. and Pandis, S. N.: *Atmospheric Chemistry and Physics*, Wiley, 2006.

782 | Spracklen, D. V., Carslaw, K. S., Pöschl, U., Rap, A. and Forster, P. M.: Global cloud condensation  
783 | nuclei influenced by carbonaceous combustion aerosol, *Atmos. Chem. Phys.*, 11(17), 9067–9087,  
784 | doi:10.5194/acp-11-9067-2011, 2011.

- 785 | [Stein, A. F., Draxler, R. R., Rolph, G. D., Stunder, B. J. B., Cohen, M. D. and Ngan, F.: NOAA's](#)  
786 | [HYSPLIT Atmospheric Transport and Dispersion Modeling System, \*Bull. Am. Meteorol. Soc.\*,](#)  
787 | [96\(12\), 2059–2077, doi:10.1175/BAMS-D-14-00110.1, 2015.](#)
- 788 | Stevens, R. G. and Pierce, J. R.: A parameterization of sub-grid particle formation in sulfur-rich plumes  
789 | for global- and regional-scale models, *Atmospheric Chemistry and Physics*, 13, 12 117-12 133,  
790 | doi:10.5194/acp-13-12117-2013, 2013.
- 791 | Stevens, R. G. and Pierce, J. R.: The contribution of plume-scale nucleation to global and regional  
792 | aerosol and CCN concentrations: evaluation and sensitivity to emissions changes, *Atmospheric*  
793 | *Chemistry and Physics Discussions*, 14, 21 473 - 21 521, doi:10.5194/acpd-14-21473-2014, 2014.
- 794 | Stevens, R. G., Pierce, J. R., Brock, C. A., Reed, M. K., Crawford, J. H., Holloway, J. S., Ryerson, T.  
795 | B., Huey, L. G., and Nowak, J. B.: Nucleation and growth of sulfate aerosol in coal-powered  
796 | power plant plumes: sensitivity to background aerosol and meteorology, *Atmospheric Chemistry*  
797 | *and Physics*, 12, 189 - 206, doi:10.5194/acp-12-189-2012, 2012.
- 798 | Stuart, G. S., Stevens, R. G., a. I. Partanen, Jenkins, a. K. L., Korhonen, H., Forster, P. M., Spracklen,  
799 | D. V., and Pierce, J. R.: Reduced efficacy of marine cloud brightening geoengineering due to in-  
800 | plume aerosol coagulation: parameterization and global implications, *Atmospheric Chemistry and*  
801 | *Physics*, 13, 10 385-10 396, doi:10.5194/acp-13-10385-2013, 2013.
- 802 | [Vakkari, V., Veli-Matti, K., Beukes, J.P., Tiitta, P., van Zyl, P.G., Josipovic, M., Venter, A.D., Jaars, K.,](#)  
803 | [Worsnop, D.R., Kulmala, M. and Laakso, L.: Rapid changes in biomass burning aerosols by](#)  
804 | [atmospheric oxidation, \*Geophys. Res. Lett.\*, 2644–2651, doi:10.1002/2014GL059396, 2014.](#)
- 805 | Van der Werf, G. R., Randerson, J. T., Giglio, L., Collatz, G. J., Mu, M., Kasibhatla, P. S., Morton, D.  
806 | C., DeFries, R. S., Jin, Y. and van Leeuwen, T. T.: Global fire emissions and the contribution of  
807 | deforestation, savanna, forest, agricultural, and peat fires (1997–2009), *Atmos. Chem. Phys.*,  
808 | 10(23), 11707–11735, doi:10.5194/acp-10-11707-2010, 2010.
- 809 | Whitby, E., McMurry, P., Shankar, U., and Binkowski, F. S.: Modal Aerosol Dynamics Modeling, Tech.  
810 | rep., Office of research and development U.S. environmental protection agency, 1991.
- 811 | Wiedinmyer, C., Akagi, S. K., Yokelson, R. J., Emmons, L. K., Al-Saadi, J. A., Orlando, J. J. and Soja,  
812 | A. J.: The Fire INventory from NCAR (FINN): a high resolution global model to estimate the  
813 | emissions from open burning, *Geosci. Model Dev.*, 4(3), 625–641, doi:10.5194/gmd-4-625-2011,  
814 | 2011.
- 815 | Yokelson, R. J., Crounse, J. D., Decarlo, P. F., Karl, T., Urbanski, S., Atlas, E., Campos, T. and  
816 | Shinozuka, Y.: Emissions from biomass burning in the Yucatan, *Atmos. Chem. Phys.*, 5785–5812,  
817 | 2009.
- 818
- 819

**Table 1.** Parameter ranges for each of the seven input parameters investigated in this study.

Parameter	Description	Units	Min. Value	Max. Value
$D_{pm0}$	Emission median dry diameter	nm	20	100
$\sigma_0$	Emission modal width	-	1.2	2.4
Mass Flux	Emission mass flux from fire	$\text{kg m}^{-2} \text{s}^{-1}$	$2 \times 10^{-8}$	$5 \times 10^{-6}$
Fire area	Square fire emissions area	$\text{km}^2$	1	49
Wind speed	Mean boundary-layer wind speed	$\text{m s}^{-1}$	2	20
Mixing depth	Mixing depth of aerosol layer	m	<b>150</b>	2500
Time	Time since emission	min	0	300

**Table 2.** Parameter ranges for inputs to the SAM-TOMAS model.

Parameter	Description	Units	Min. value	Max. value
Date	Req. for Met. field selection	8-hour	July 1, 2010	July 31, 2010
Latitude		deg N	30	70
Longitude		deg W	70	135
$D_{pm0}$	Emission median dry diameter	nm	20	100
$\sigma_0$	Emission modal width	-	1.2	2.4
Mass Flux	Emission mass flux from fire	$\text{kg m}^{-2} \text{s}^{-1}$	$2 \times 10^{-8}$	$5 \times 10^{-6}$
Fire area	Square fire emissions area	$\text{km}^2$	1	49
Injection height	Lower plume injection bound	m	50	150
Injection depth	Depth of plume at emission	m	500	2000

**Table 3.** Best-fit parameters for the simplified  $D_{pm}$  and  $\sigma$  SAM-TOMAS parameterizations (Eqns. 1 to 4)

Fit	Eqn. #	Parameter		
		A	b	c
$D_{pm}(dM/dx)$	(1)	4.268	0.3854	0.4915
$D_{pm}(dM/dxdz)$	(2)	84.58	0.4191	0.4870
$\sigma(dM/dx)$	(3)	0.05940	0.1915	0.3569
$\sigma(dM/dxdz)$	(4)	0.2390	0.1889	0.3540

**Table 4: Measured and calculated  $D_{pm}$  and  $\sigma$  of biomass-burning plumes observed at MBO during August 2015. For the calculated  $D_{pm}$  and  $\sigma$  of, the initial size parameters used were  $D_{pm0} = 100$  nm and  $\sigma_0 = 1.9$ .**

Plume	Plume date and time (UTC)	# fire areas	Measured (SMPS)		Calculated			
			$D_{pm}$ (nm)	$\sigma$	using $dM/dx$		using $dM/dxdz$	
			$D_{pm}$ (nm)	$\sigma$	$D_{pm}$ (nm)	$\sigma$	$D_{pm}$ (nm)	$\sigma$
1	8/9/2015 3:00-4:00	3	136.1	1.95	140.7	1.64	151.1	1.59
2	8/9/2015 5:00-7:00	3	144.0	1.77	140.8	1.64	152.0	1.58
3	8/10/2015 3:00-5:00	3	190.1	1.50	140.9	1.63	149.7	1.58
4	8/23/2015 3:55-7:00	1	162.5	1.89	145.5	1.63	162.4	1.57
5	8/24/2015 4:00-7:25	1	201.1	1.59	167.5	1.55	184.7	1.49
6	8/24/2015 7:30-11:20	1	217.5	1.52	190.1	1.50	230.1	1.40
7	8/24/2015 13:00-18:00	1	212.5	1.49	193.9	1.48	237.8	1.37
8	8/25/2015 3:50-6:50	1	192.2	1.54	161.4	1.57	172.6	1.52
9	8/27/2015 9:00-13:00	3	192.9	1.50	194.2	1.49	220.6	1.43
10	8/28/2015 8:00-11:15	3	183.4	1.54	182.1	1.50	203.2	1.43
11	8/28/2015 17:40-19:40	3	176.7	1.60	181.4	1.50	202.0	1.43



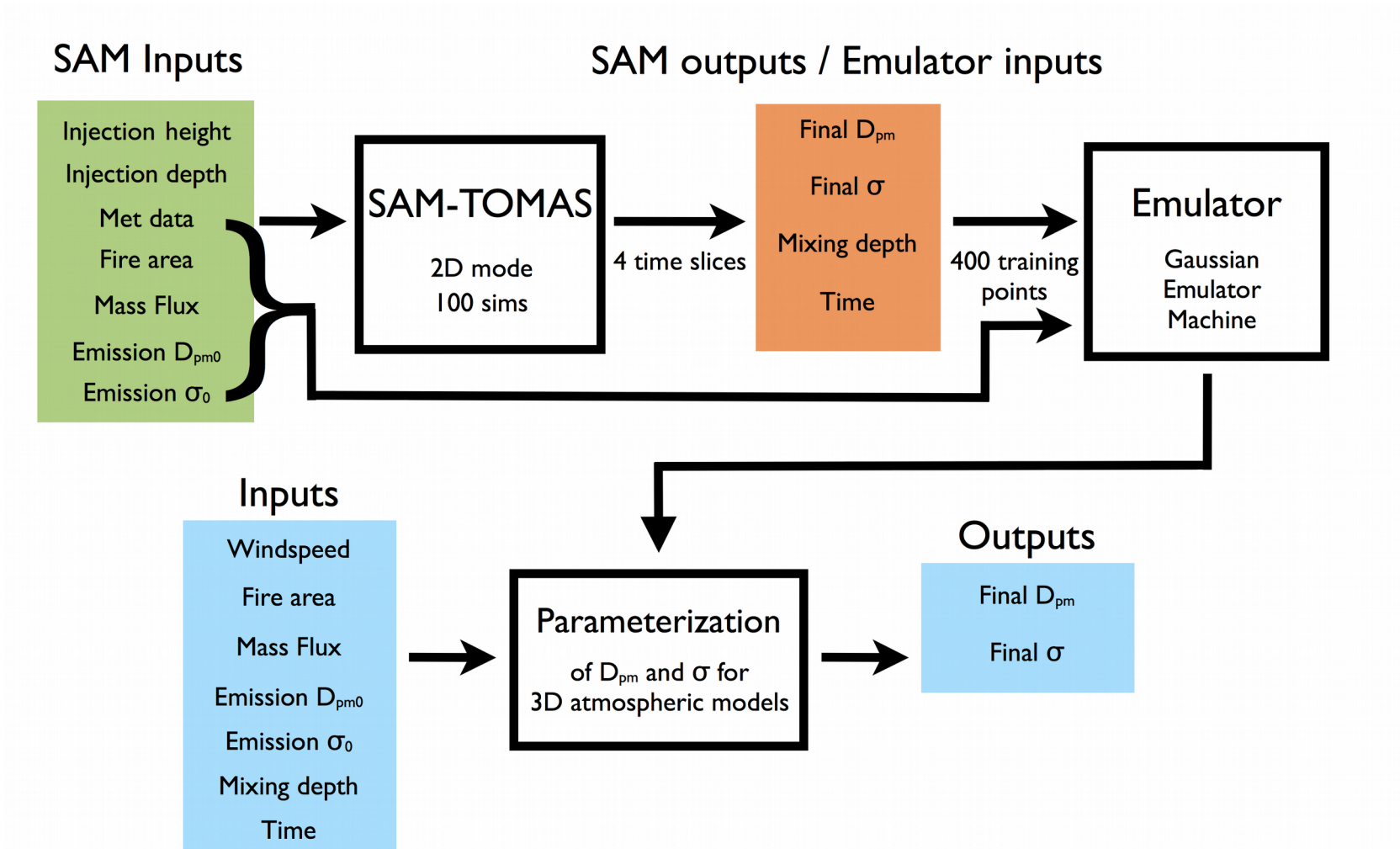


**Figure 1.** Schematic of the methods in this paper.

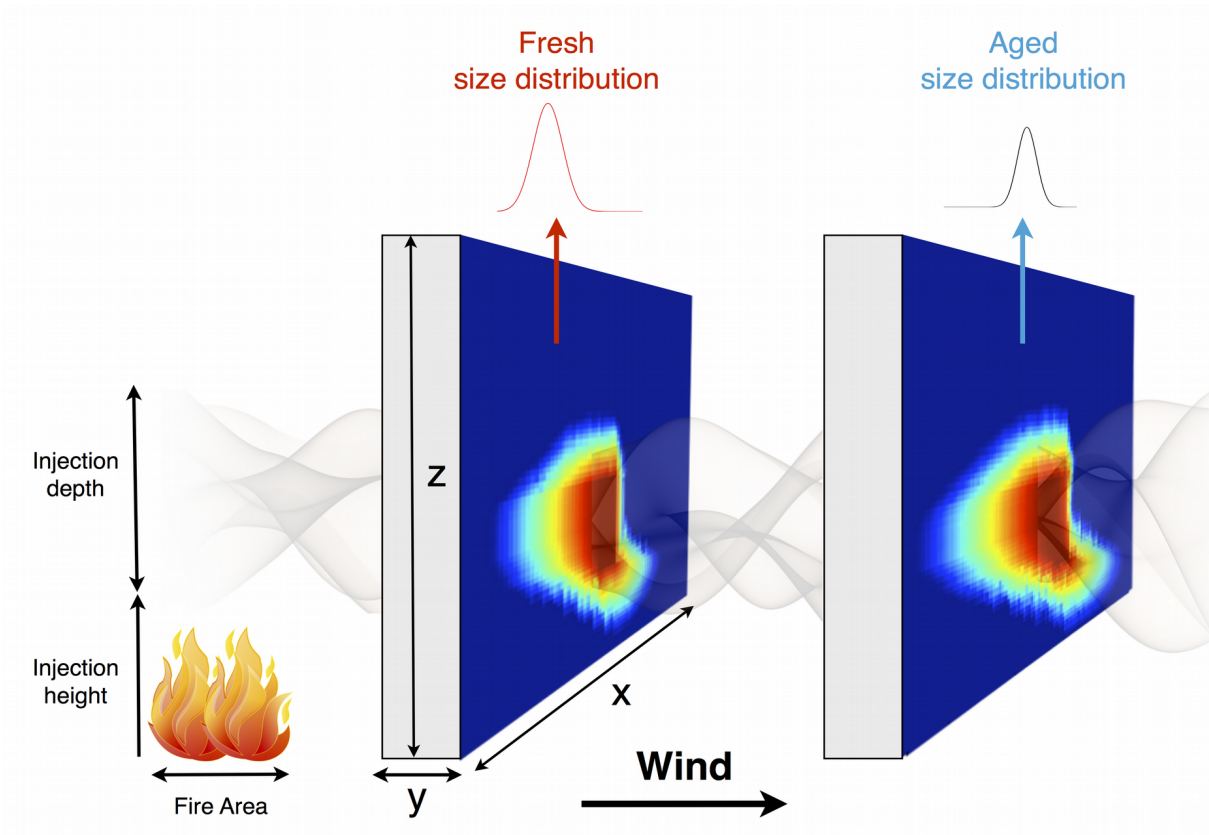


**Figure 2.** Schematic of a 2D SAM-TOMAS plume simulation.

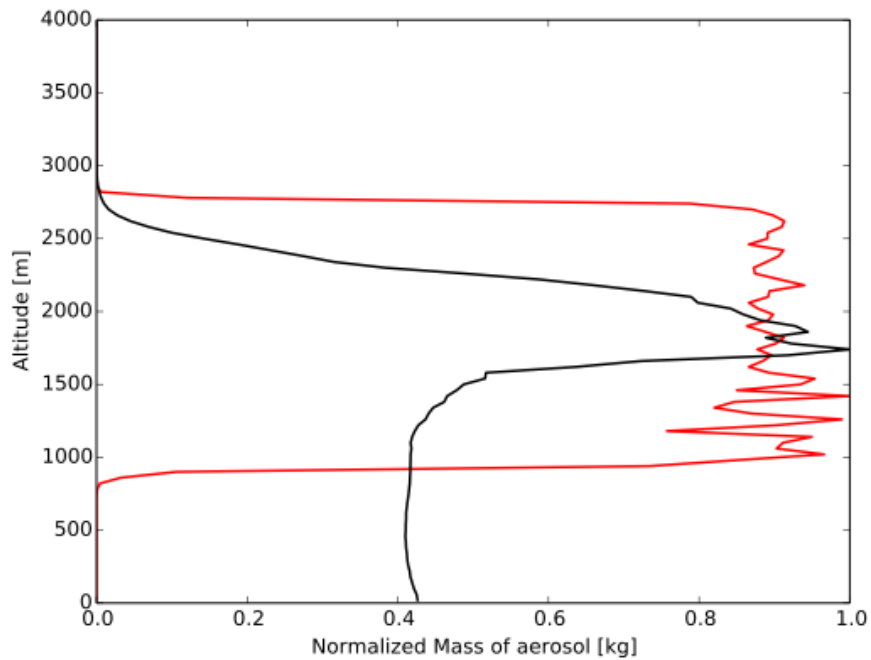


**Figure 3. Final vertical profiles for two representative SAM-TOMAS simulations after four hours, normalized to individual aerosol load and averaged horizontally across the domain. The black profile shows a simulation where the aerosol mixed through the boundary layer to the ground with some aerosol still trapped in a stable emission layer, while the red profile shows a simulation where the aerosol plume is still stable at the emission injection layer.**

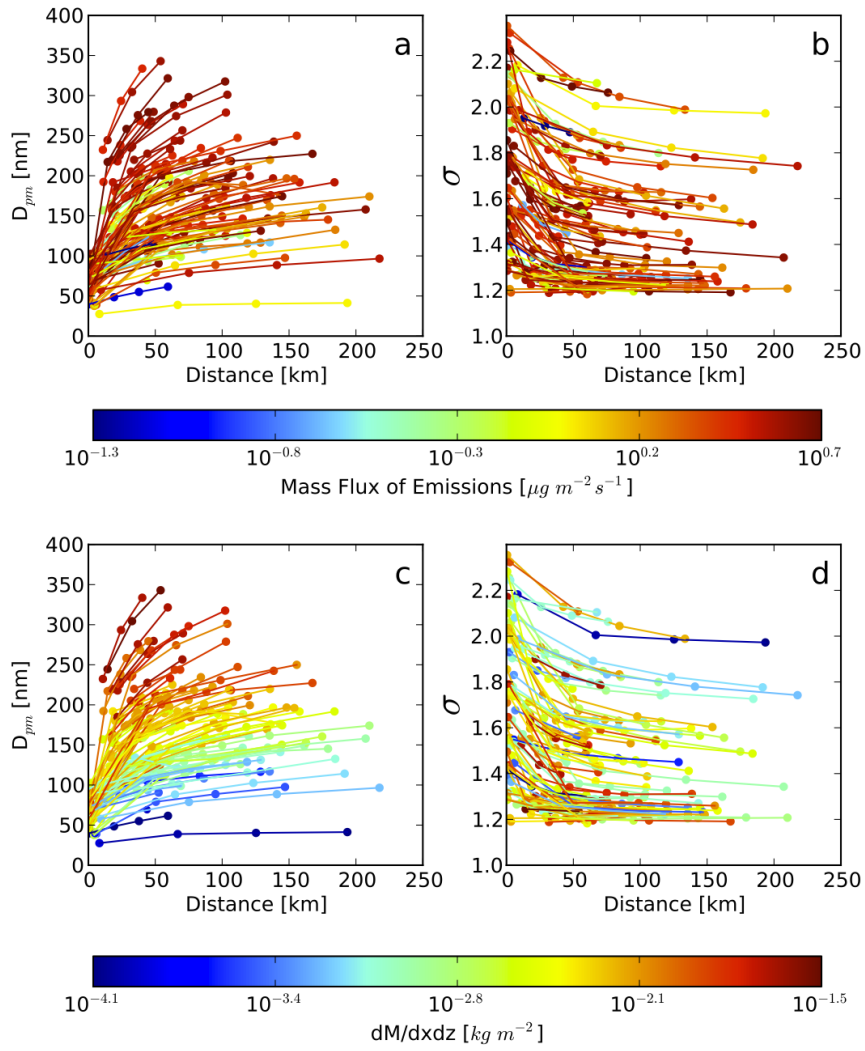


**Figure 4.** Wire plots showing size-distribution changes across individual SAM-TOMAS simulations colored by emission mass flux (panels a and b) and  $dM/dxdz$  (panels c and d) for  $D_{pm}$  (panels a and c) and  $\sigma$  (panels b and d).

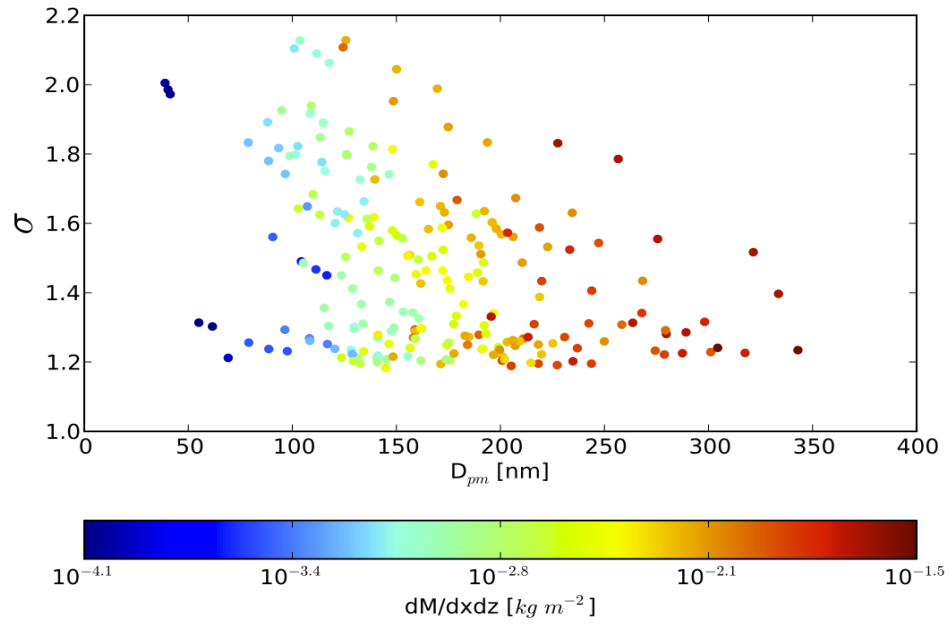


**Figure 5.** Scatter plot showing the relationships between final modal width ( $\sigma$ ), final  $D_{pm}$ , and  $dM/dxdz$  for each of the SAM-TOMAS simulation slices at distances greater than 25 km from the fire.

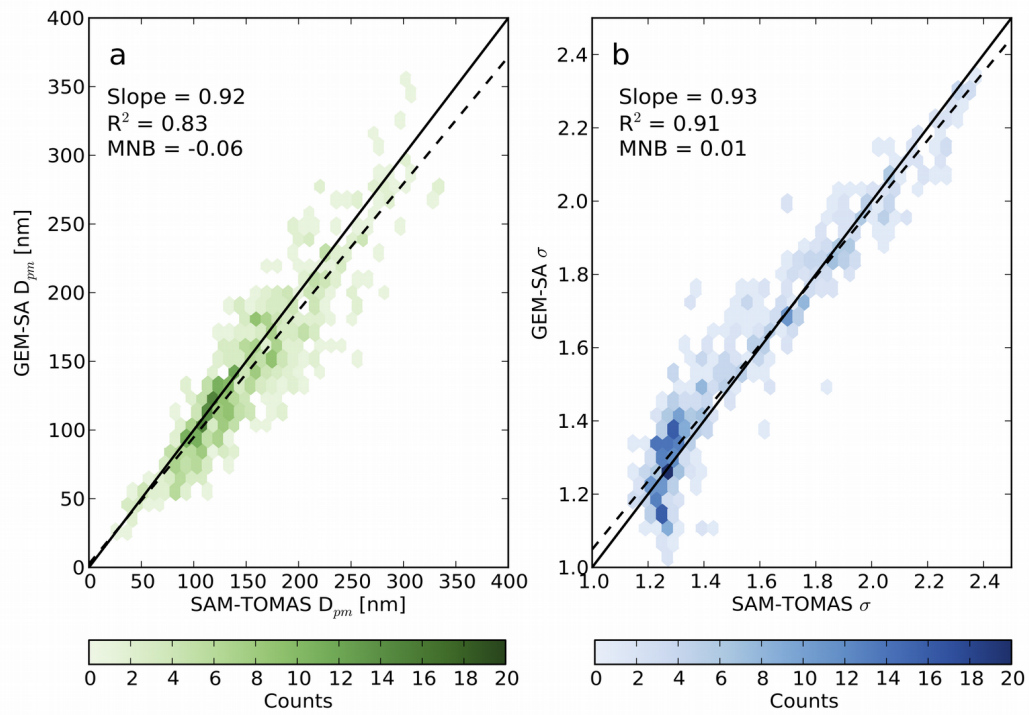


**Figure 6.** One-to-one plots showing GEM-SA emulator vs. SAM-TOMAS for 624 non-training simulation slices for a) final  $D_{pm}$ , and b) final modal width,  $\sigma$ . The black line is the one-to-one line. The dashed black line is the line of best fit.

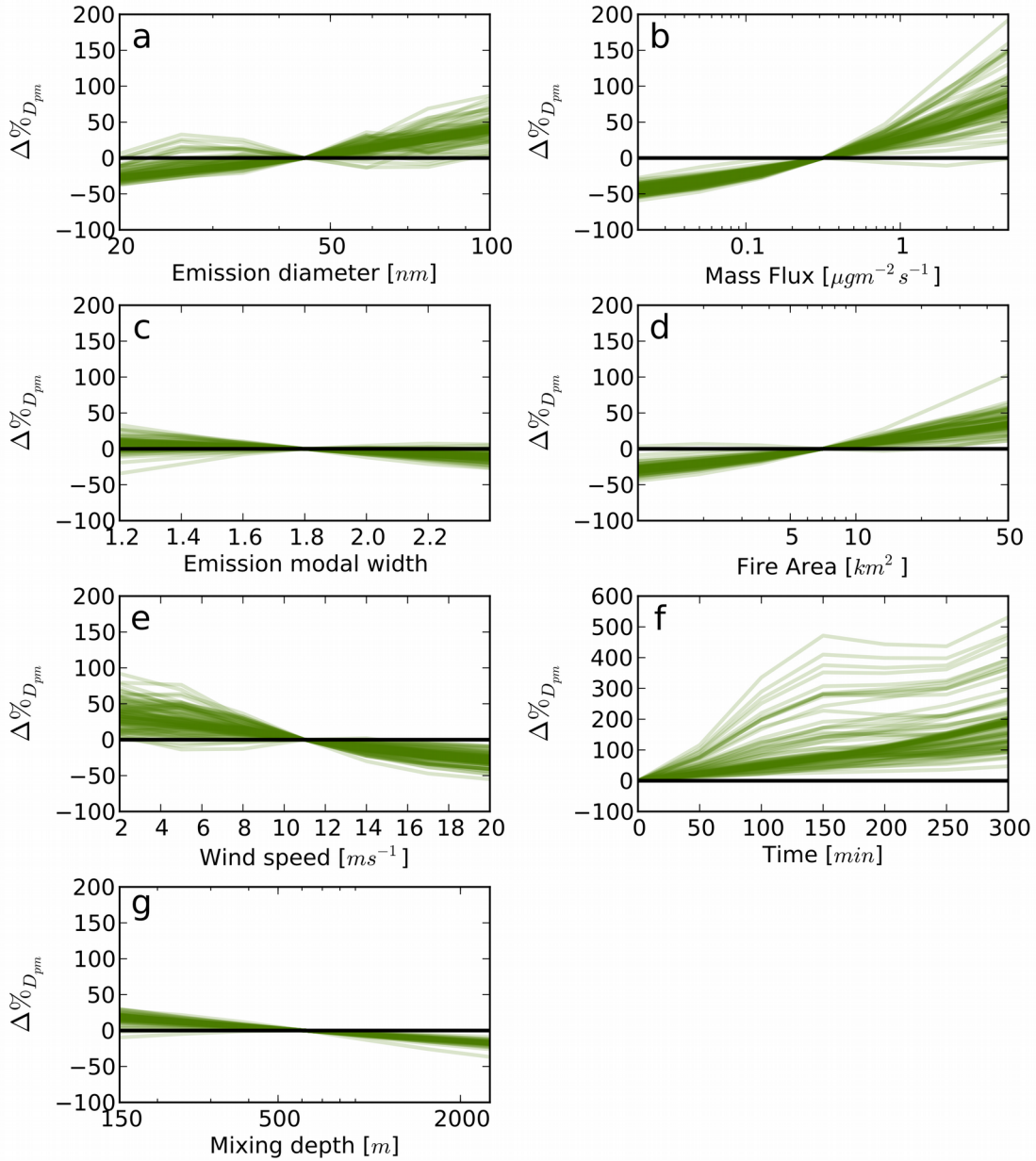


**Figure 7.** Sensitivity plots for the seven input parameters to the GEM-SA  $D_{pm}$  parameterization. For each panel, a single input parameter is varied systematically from its minimum to maximum value for 100 randomly chosen sets of the other six parameters (100 lines in each panel). The sensitivities are shown as percent change in final  $D_{pm}$ , individually normalized to the value at the center of the x-axis (to zero in Time).

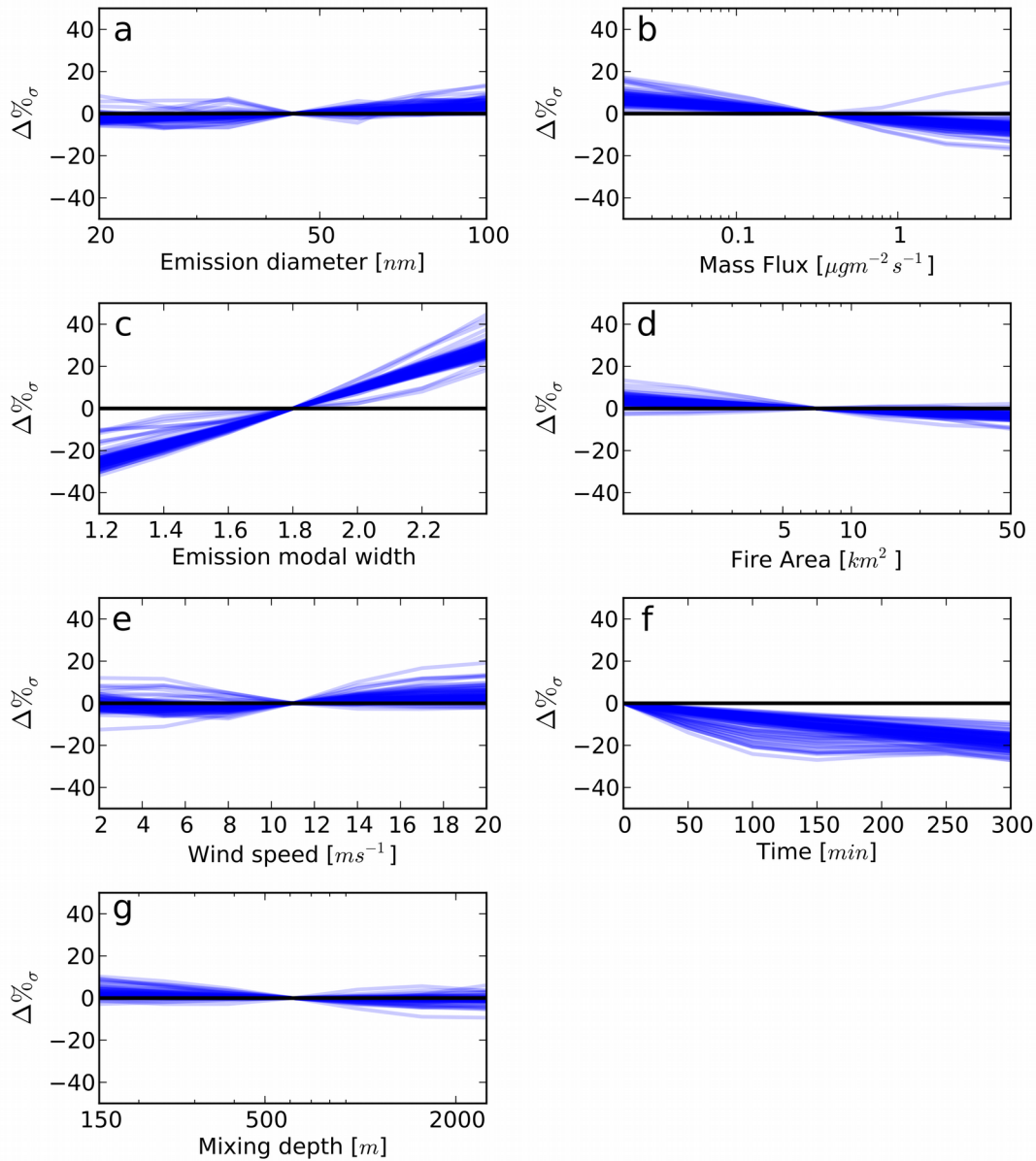


**Figure 8.** Sensitivity plots for the seven input parameters to the GEM-SA  $\sigma$  emulator parameterization. For each panel, a single input parameter is varied systematically from its minimum to maximum value for 100 randomly chosen sets of the other six parameters (100 lines in each panel). The sensitivities are shown as percent change in final  $\sigma$ , individually normalized to the center value of the x-axis (to zero in Time).



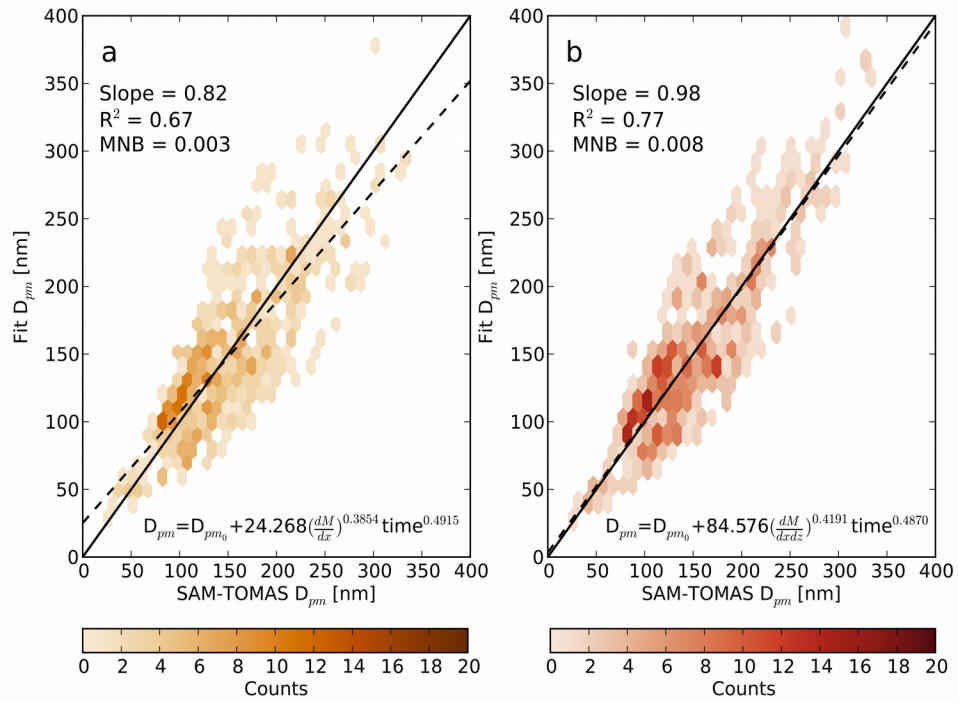


**Figure 9.** One-to-one plot showing simplified  $D_{pm}$  fits vs SAM-TOMAS for a)  $dM/dx$ , and b)  $dM/dxdz$ . The black line is the one-to-one line. The dashed black line is the line of best fit.  $N = 624$ .

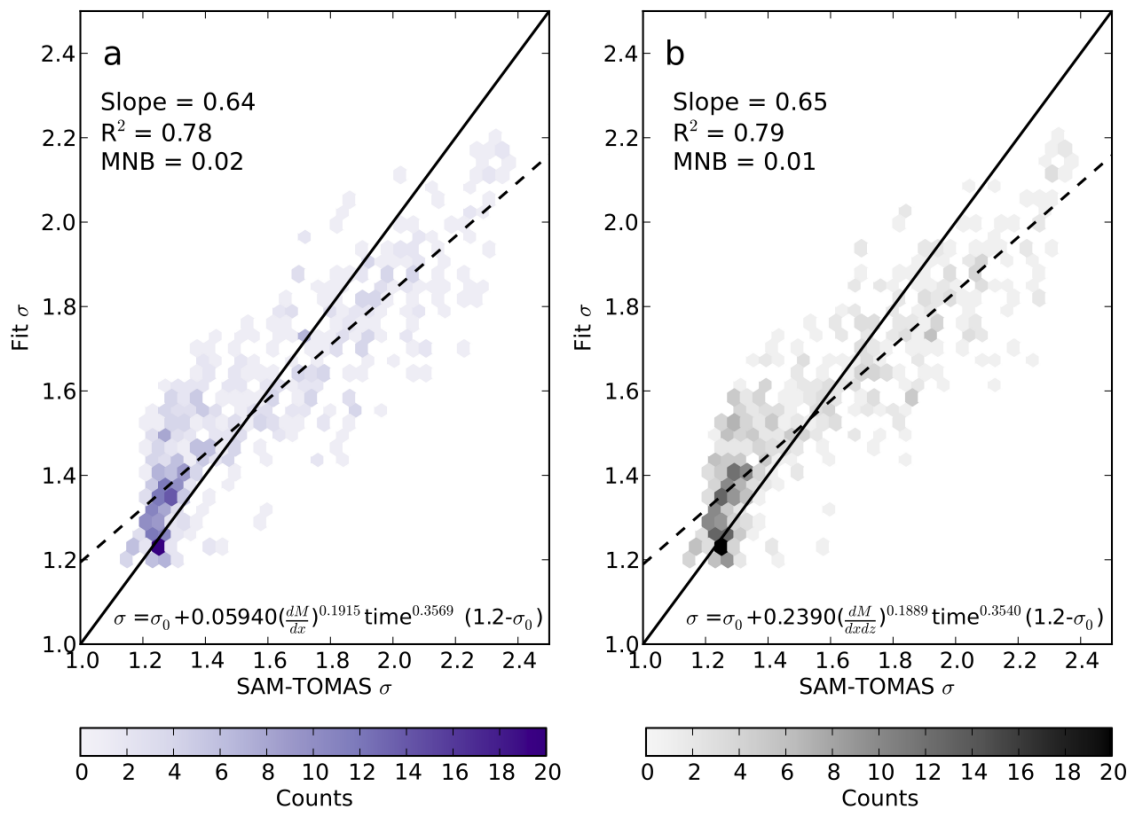


**Figure 10.** One-to-one plot showing simplified  $\sigma$  fits vs SAM-TOMAS for a)  $dM/dx$ , and b)  $dM/dxdz$ . The solid black line is the one-to-one line. The dashed black line is the line of best linear fit.  $N = 624$ .

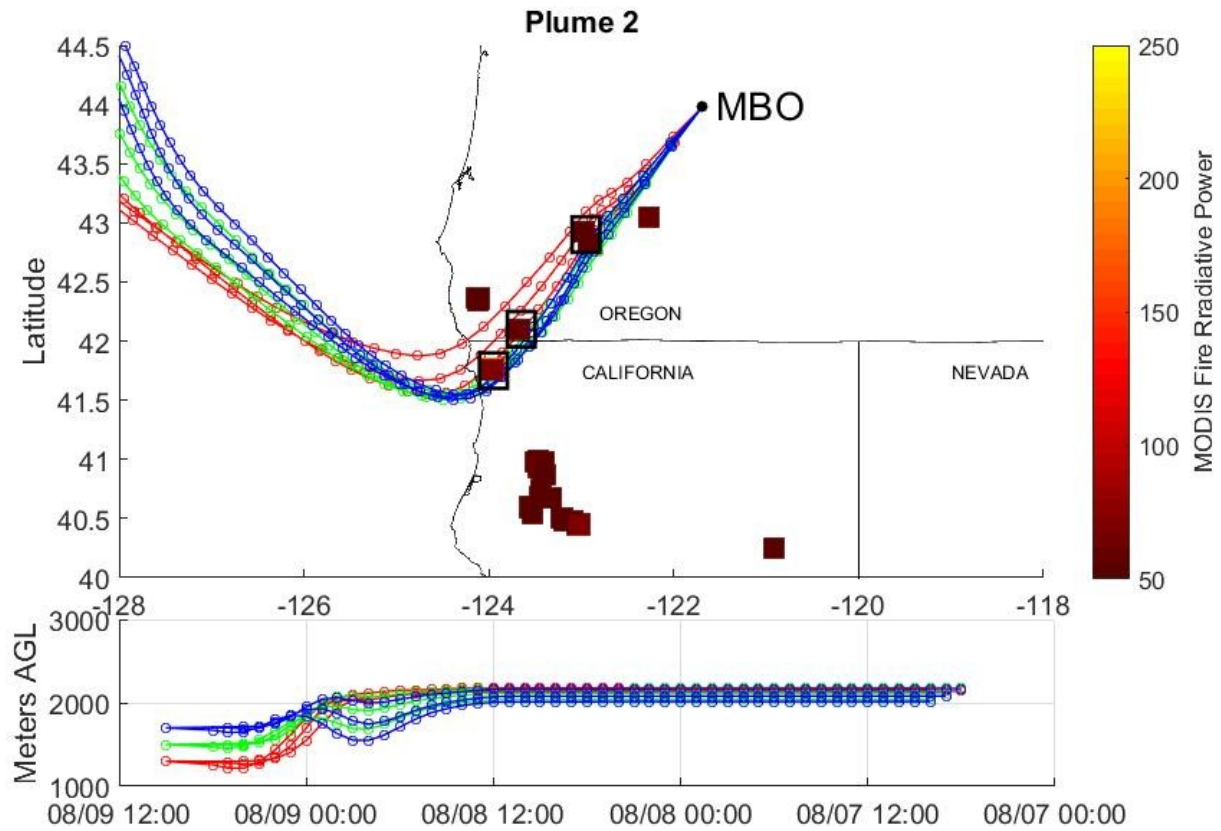


**Figure 11. Back-trajectories from plume 2 observed at MBO. The colored squares represent fires during the time of the back-trajectory and are colored by Fire Radiative Power (FRP). The black squares indicate the fire areas used in the parameterization to estimate  $D_{pm}$  and  $\sigma$ .**

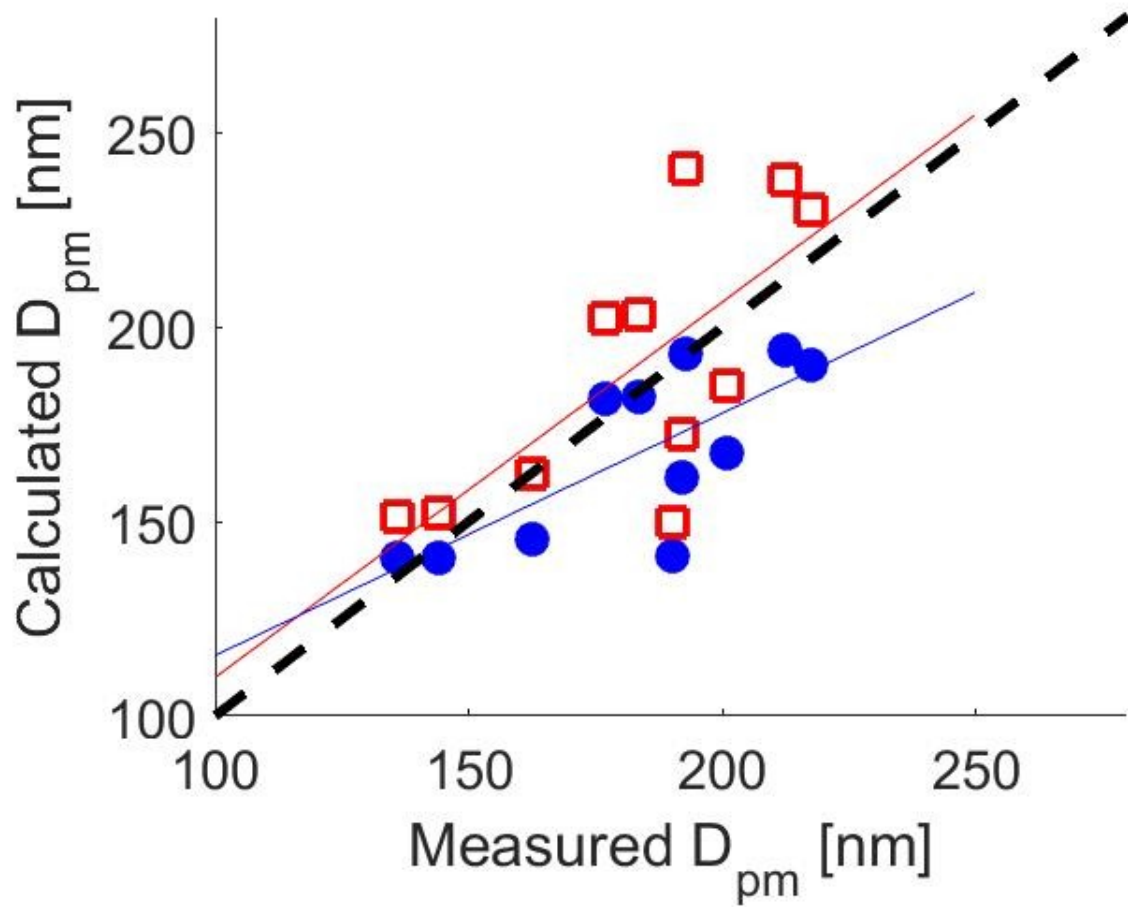
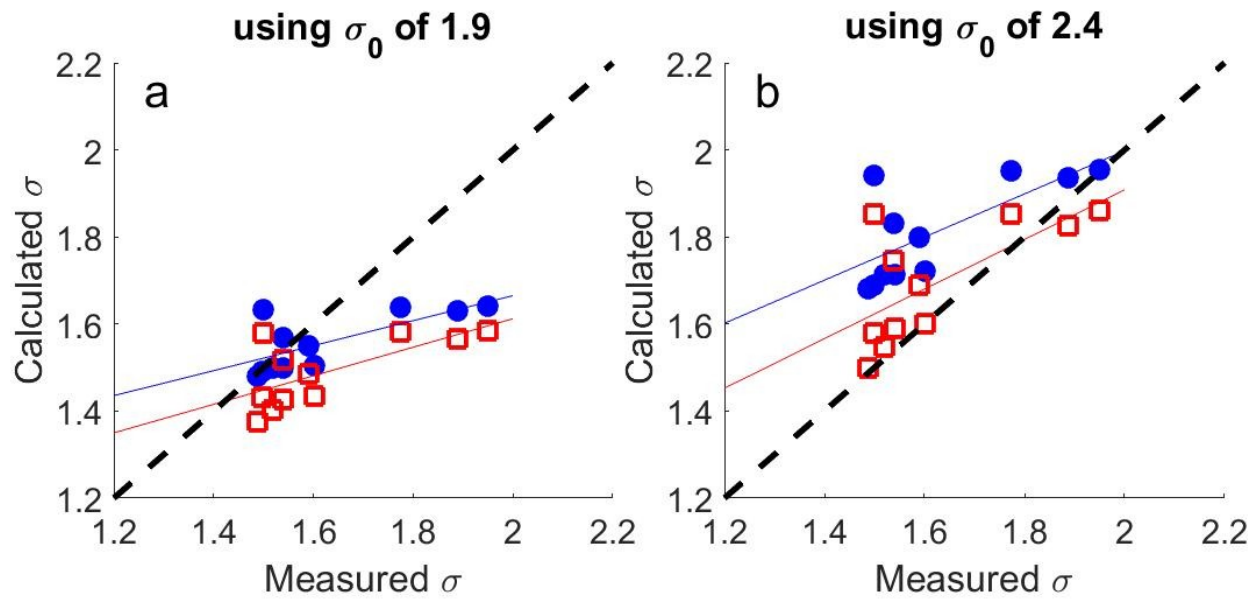


Figure 12. Scatter plot showing calculated and measured  $D_{pm}$  for biomass-burning plumes observed at MBO during August of 2015. The blue circles represent  $D_{pm}$  calculated using Eqn. 1 ( $dM/dx$ ), and the red circles represent  $D_{pm}$  calculated using Eqn. 2 ( $dM/dxdz$ ).



**Figure 13. Scatter plots showing calculated and measured modal width ( $\sigma$ ) for biomass-burning plumes observed at MBO during August of 2015. The blue circles represent  $\sigma$  calculated using Eqn. 3 ( $dM/dx$ ), and the red circles represent  $\sigma$  calculated using Eqn 4. ( $dM/dxdz$ ). Different emission modal width values ( $\sigma_0$ ) were used to calculate  $\sigma$ , (a) used a  $\sigma_0$  of 1.9 and (b) used a  $\sigma_0$  of 2.4.**